Cingulo-Opercular Control Network Supports Disused Motor Circuits in Standby Mode

Authors:
Dillan J. Newbold[1,*], Evan M. Gordon[2], Timothy O. Laumann[3], Nicole A. Seider[1], David F. Montez[1,3], Sarah J. Gross[1], Annie Zheng[1], Ashley N. Nielsen[1,4], Catherine R. Hoyt[5], Jacqueline M. Hampton[3], Mario Ortega[1], Babatunde Adeyemo[1], Derek B. Miller[1], Andrew N. Van[1,6], Scott Marek[1], Bradley L. Schlaggar[7,8,9], Alexandre R. Carter[1,5], Benjamin P. Kay[1], Deanna J. Greene[2,3], Marcus E. Raichle[1,2], Steven E. Petersen[1,2,6,10,11], Abraham Z. Snyder[1,2], Nico U.F. Dosenbach[1,2,5,6,12,*]

Affiliations:
[1]Department of Neurology, Washington University School of Medicine, St. Louis, MO 63110, USA.
[2]Department of Radiology, Washington University School of Medicine, St. Louis, MO 63110, USA.
[3]Department of Psychiatry, Washington University School of Medicine, St. Louis, MO 63110, USA.
[4]Institute for Innovations in Developmental Sciences, Northwestern University, Chicago, IL 60611, USA.
[5]Program in Occupational Therapy, Washington University School of Medicine, St. Louis, MO 63110, USA.
[6]Department of Biomedical Engineering, Washington University in St. Louis, St. Louis, MO 63110, USA.
[7]Kennedy Krieger Institute, Baltimore, MD 21205, USA.
[8]Department of Neurology, Johns Hopkins University School of Medicine, Baltimore, MD 21287, USA.
[9]Department of Pediatrics, Johns Hopkins University School of Medicine, Baltimore, MD 21287, USA.
[10]Department of Neuroscience, Washington University School of Medicine, St. Louis, MO 63110, USA.
[11]Department of Psychological and Brain Sciences, Washington University in St. Louis, St. Louis, MO 63110, USA.
[12]Department of Pediatrics, Washington University School of Medicine, St. Louis, MO 63110, USA.
*Correspondence: newbold@wustl.edu, dosenbachn@wustl.edu

Abstract

Two weeks of upper extremity casting induced plasticity beyond somatomotor regions. Whole-brain resting-state functional MRI (rs-fMRI) revealed that disused motor regions became more strongly connected to the cingulo-opercular network (CON), an executive control network that includes regions of the dorsal anterior cingulate cortex (dACC) and insula. Disuse-driven increases in functional connectivity (FC) were specific to the CON and somatomotor networks and did not involve any other networks, such as the salience, frontoparietal or default mode networks. FC increases during casting were mediated by large, spontaneous activity pulses that appeared in disused motor regions and network-adjacent CON control regions. During limb constraint, disused motor circuits appear to enter a standby mode characterized by spontaneous activity pulses and strengthened connectivity to CON executive control regions.

Introduction

Disuse is a powerful paradigm for inducing plasticity that has uncovered key organizing principles of the human brain[1-4]. Monocular deprivation revealed that multiple afferent inputs can compete for representational territory in the primary visual cortex[1]. Competition between afferents also shapes the somatomotor system, and manipulations such as peripheral nerve deafferentation, whisker trimming, and limb constraint all drive plasticity in the primary somatosensory and motor cortex[2-4]. Most plasticity studies to date have used focal techniques, such as microelectrode recordings, to study local changes in brain function. As a result, little is known about how behavior and experience shape brain-wide functional networks.

The brain is composed of networks of regions that cooperate to perform specific cognitive operations[5-7]. These functional networks show synchronized spontaneous activity while the brain is at rest, a phenomenon known as resting state functional connectivity (FC)[8-10]. FC can be measured non-invasively in humans using resting-state functional MRI (rs-fMRI). Whole-brain rs-fMRI has been used to parse the brain into canonical functional networks[11,12], including visual, auditory and somatomotor networks[13,14]; ventral and dorsal attention networks[7,15]; a default mode network with roles in internally directed cognition and episodic memory[6,10]; a salience network thought to assess the homeostatic relevance of external stimuli[16]; a frontoparietal control network supporting error-processing and moment-to-moment adjustments in behavior[17-19]; and a cingulo-opercular control network (CON), which maintains executive control during goal-directed behavior[17,18,20].

A more recent advance in human neuroscience has been the recognition of individual variability in network organization[21-24]. Most early rs-fMRI studies examined central tendencies in network organization using group-averaged FC measurements[9,11,12]. Recent work has

demonstrated that functional networks can be described in an individual-specific manner if sufficient rs-fMRI data are acquired, an approach termed Precision Functional Mapping (PFM)[21,22,25-29]. PFM respects the unique functional anatomy of each person and avoids averaging together functionally distinct brain regions across individuals.

We recently demonstrated that PFM can track disuse-driven plasticity in the human brain[30]. Three adult participants (P1, P2 and P3) were scanned at the same time every day for 42-64 consecutive days (30 minutes of rs-fMRI/day) before, during and after two weeks of dominant upper extremity casting (Fig. 1a-b). During casting, the upper-extremity regions of the primary somatomotor cortex (L-SM1$_{ue}$) and cerebellum

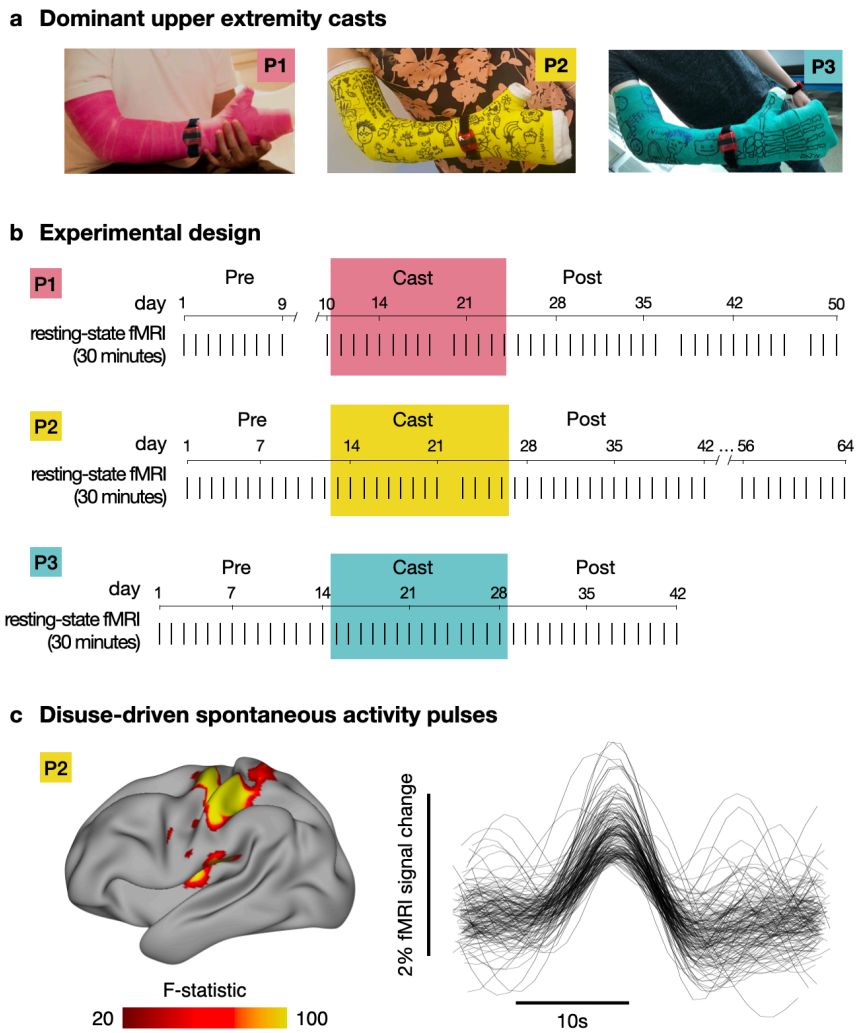

Fig. 1 | Experimental Design and Spontaneous Activity Pulses. a, Three participants (P1, P2 and P3) wore casts covering the entire dominant upper extremity for two weeks. **b,** Participants were scanned every day for 42-64 consecutive days before, during and after casting. All scans included 30 minutes of resting-state functional MRI (rs-fMRI). **c,** During the cast period, disused somatomotor circuits exhibited spontaneous activity pulses[30].

60 (R-Cblm$_{ue}$) functionally disconnected from the remainder of the somatomotor network. Disused
61 motor circuits also exhibited large, spontaneous pulses of activity (Fig. 1c).
62
63 Somatomotor circuits do not function in isolation. Action selection and motor control are
64 thought to be governed by complex interactions between the somatomotor network and control
65 networks, including the CON[17]. Here, we leveraged the whole-brain coverage of rs-fMRI to
66 examine disuse-driven plasticity beyond the somatomotor system. We first examined disuse-
67 driven changes in FC between L-SM1$_{ue}$ and the remainder of the cerebral cortex. We then
68 performed comprehensive analyses of FC changes between all pairs of individual-specific
69 cortical, subcortical and cerebellar parcels (>200,000 possible connections). Finally, we tested
70 if observed changes in FC could be explained by the occurrence of spontaneous activity
71 pulses during the cast period.
72

73 ## Results

74 **Disuse Caused Both Increases and Decreases in Functional Connectivity**

75 To examine disuse-driven plasticity beyond somatomotor networks, we first generated seed
76 maps showing FC between L-SM1$_{ue}$ and all other cortical regions before, during and after
77 casting (Fig. 2a, Supplementary Fig. 1). Prior to casting (Pre), L-SM1$_{ue}$ was strongly connected
78 to the remainder of the somatomotor cortex (pre- and post-central gyri), especially homotopic
79 R-SM1$_{ue}$. During the cast period (Cast), L-SM1$_{ue}$ showed a new pattern of connectivity, with
80 strong connections to bilateral secondary somatosensory cortex (SII), dorsal anterior cingulate
81 cortex (dACC), and pre- and post-central sulci. After casting (Post), L-SM1$_{ue}$ FC returned to
82 baseline. Changes in FC during casting (Cast – Pre) and recovery (Post – Cast) were
83 examined using sets of previously published individual-specific cortical parcels[21,30]. Casting
84 caused decreased L-SM1$_{ue}$ connectivity with the remainder of the somatomotor cortex, as well

as increased connectivity with the bilateral SII, dACC, and pre- and post-central sulci (Fig. 2b, Supplementary Fig. 1). FC changes after cast removal were strongly negatively correlated with changes during casting (P1: spatial correlation, $r = -0.56$, $P < 0.001$; P2: $r = -0.95$, $P < 0.001$; P3: $r = -0.32$, $P < 0.001$), indicating that most effects reversed after cast removal (Fig. 2b, Supplementary Fig. 1).

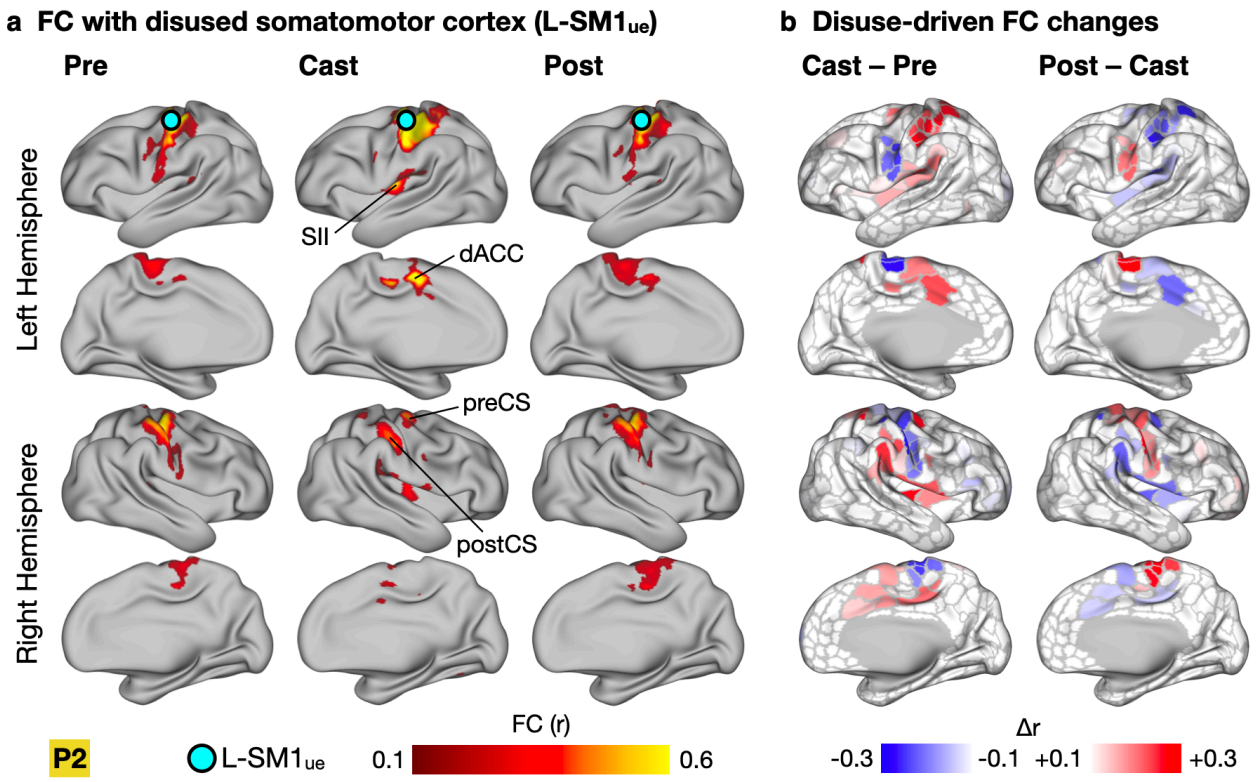

Fig. 2 | Cast-driven Changes in Functional Connectivity (FC) of Disused Somatomotor Cortex (L-SM1$_{ue}$). a, Seed maps showing FC between L-SM1$_{ue}$ and the remainder of the cerebral cortex in an example participant (P2; remaining participants, Supplementary Fig. 1). Seed maps were averaged across sessions before, during and after casting (Pre, Cast, Post). Labels indicate secondary somatosensory cortex (SII), dorsal anterior cingulate cortex (dACC), and pre- and post-central sulci (preCS and postCS). **b,** Subtraction maps showing changes in FC during casting (Cast – Pre) and recovery (Post – Cast). Differences are shown on a set of previously published individual-specific cortical parcels[21].

Disuse-driven Functional Connectivity Changes Were Highly Focal in Network Space

The brain's functional network organization can be visualized using spring-embedded graphs, which treat functional connections as spring forces, positioning more strongly connected nodes closer to one another (Fig. 3a, Supplementary Fig. 2). While L-SM1$_{ue}$ FC increases were

distributed in anatomical space, including regions on the medial and lateral surfaces of both hemispheres, nearly all of these changes mapped onto a single cluster in network space, the

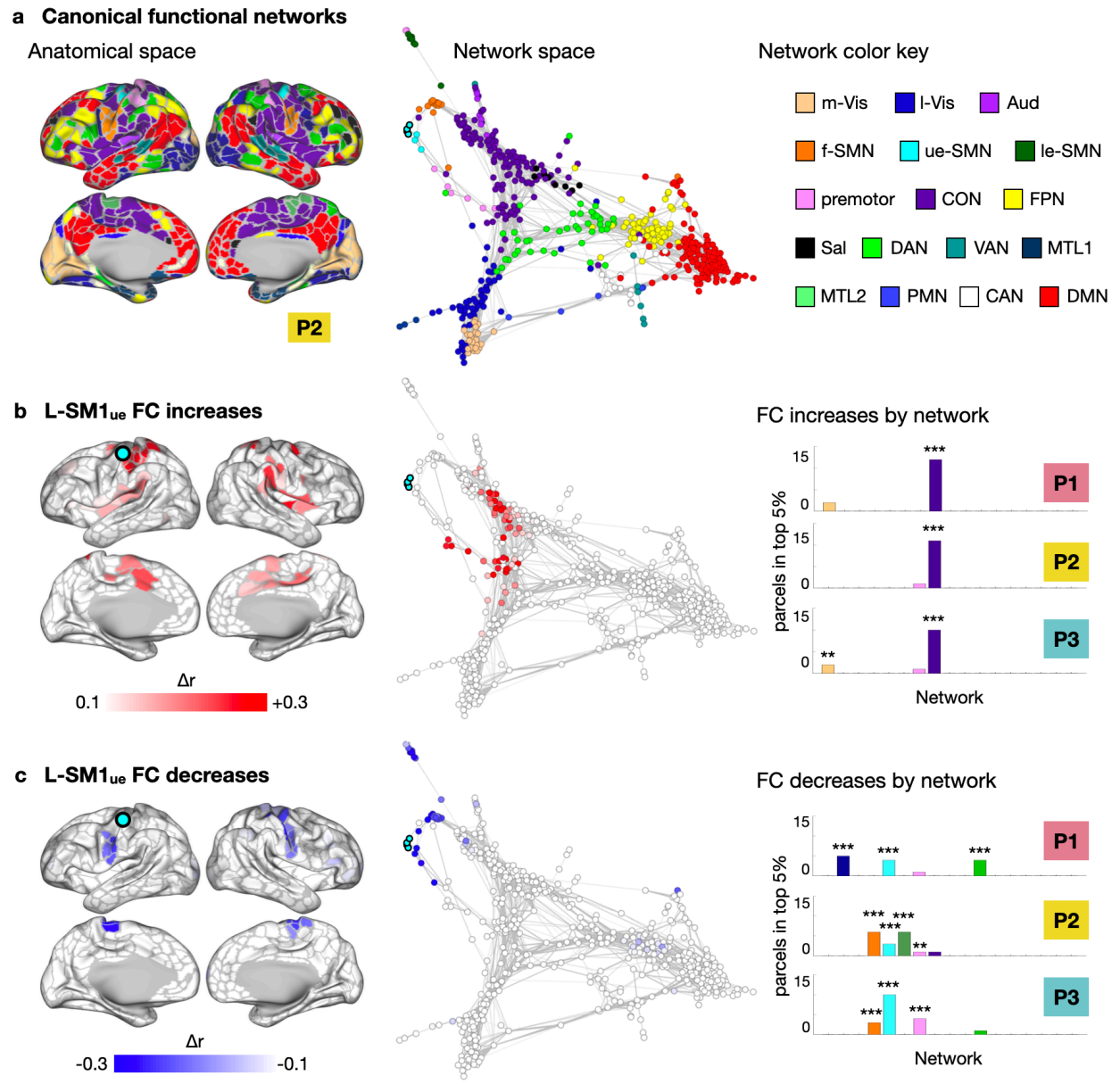

Fig. 3 | Disused Somatomotor Cortex (L-SM1$_{ue}$) Functional Connectivity (FC) Changes in Network Space. a, Map of canonical functional networks in an example participant (P2; remaining participants, Supplementary Fig. 2). *Left:* Networks shown in anatomical space (inflated cortical surfaces). *Middle:* Same map as *Top*, shown in network space (spring-embedded graphs based on Pre scans). *Right:* Network color key: m-Vis: medial visual; l-Vis: lateral visual; Aud: auditory; f-SMN: face somatomotor; ue-SMN: upper-extremity somatomotor; le-SMN: lower-extremity somatomotor; CON: cingulo-opercular; FPN: fronto-parietal; Sal: salience; DAN: dorsal attention; VAN: ventral attention; MTL: medial temporal lobe; PMN: parietal memory; CAN: context association; DMN: default mode. **b,** *Left:* Subtraction maps showing disuse-driven decreases in functional connectivity (FC) with left somatomotor cortex (L-SM1$_{ue}$) in anatomical space. *Middle:* Same map as *Top,* shown in network space. *Right:* Distribution of top 5% FC decreases across all networks. **P < 0.01; ***P < 0.001; FDR < 0.05. **c,** Subtraction maps showing disuse-driven increases in FC with L-SM1$_{ue}$ in anatomical (*Left*) and network space (*Middle*). *Right:* Distribution of top 5% FC increases across all networks.

97 CON (Fig. 3b, Supplementary Fig. 2). The network focality of L-SM1$_{ue}$ FC increases was
98 quantified by examining the distribution of the greatest FC increases (top 5%) across the
99 canonical functional networks (Fig. 3b). In all participants, the CON showed more FC
100 increases than expected by chance ($P < 0.001$ for all participants). Decreases in L-SM1$_{ue}$ FC
101 were also localized in network space (Fig. 3c, Supplementary Fig. 2). Most of the regions
102 showing decreased FC with L-SM1$_{ue}$ during casting belonged to the somatomotor networks
103 (ue-SMN, le-SMN, face-SMN and premotor). All participants showed more FC decreases than
104 expected by chance in the upper-extremity somatomotor network (ue-SMN; $P < 0.001$ for all
105 participants). Additionally, two participants (P2 and P3) showed significant FC decreases in
106 other somatomotor networks, including the lower-extremity and face somatomotor networks
107 (le-SMN and f-SMN) and the premotor network.
108
109 **Plasticity Was Restricted to the Somatomotor and Cingulo-opercular Networks**
110 The analyses presented thus far focus on changes in connectivity between L-SM1$_{ue}$ and the
111 remainder of the cerebral cortex. To examine whole-brain patterns of FC changes induced by
112 casting, we extracted rs-fMRI signals from individual-specific cortical, subcortical and
113 cerebellar parcels (P1: 744 parcels, P2: 733; P3: 761) and examined FC changes in all
114 possible pairwise connections (Supplementary Fig. 3). We displayed the 50 largest changes in
115 FC (25 greatest increases and 25 greatest decreases) in anatomical space (Fig. 4a,
116 Supplementary Fig. 3). Disuse-driven FC changes involved L-SM1$_{ue}$ more than expected by
117 chance (P1: 9/50 connections, $P = 0.018$; P2: 37/50, $P < 0.001$; P3: 39/50, $P < 0.001$). Figure

4b shows the total magnitude of whole-brain FC change for each vertex/voxel. The total magnitude of whole-brain FC change was significantly greater in L-SM1$_{ue}$ than in the remainder of the brain (Fig. 4B, Supplementary Fig. 3; P1: $P = 0.021$; P2: $P < 0.001$; P3: $P = 0.005$).

Increased Somatomotor Connectivity with the CON Depended on a Recent History of Disuse

To distinguish between increases in connectivity due to wearing a cast during MRI scans (i.e., an altered behavioral state) and increases in connectivity due to a history of having been casted (i.e., disuse-driven plasticity), we conducted a control experiment in which participants wore casts during 30-minute scans but were not casted during their daily lives.

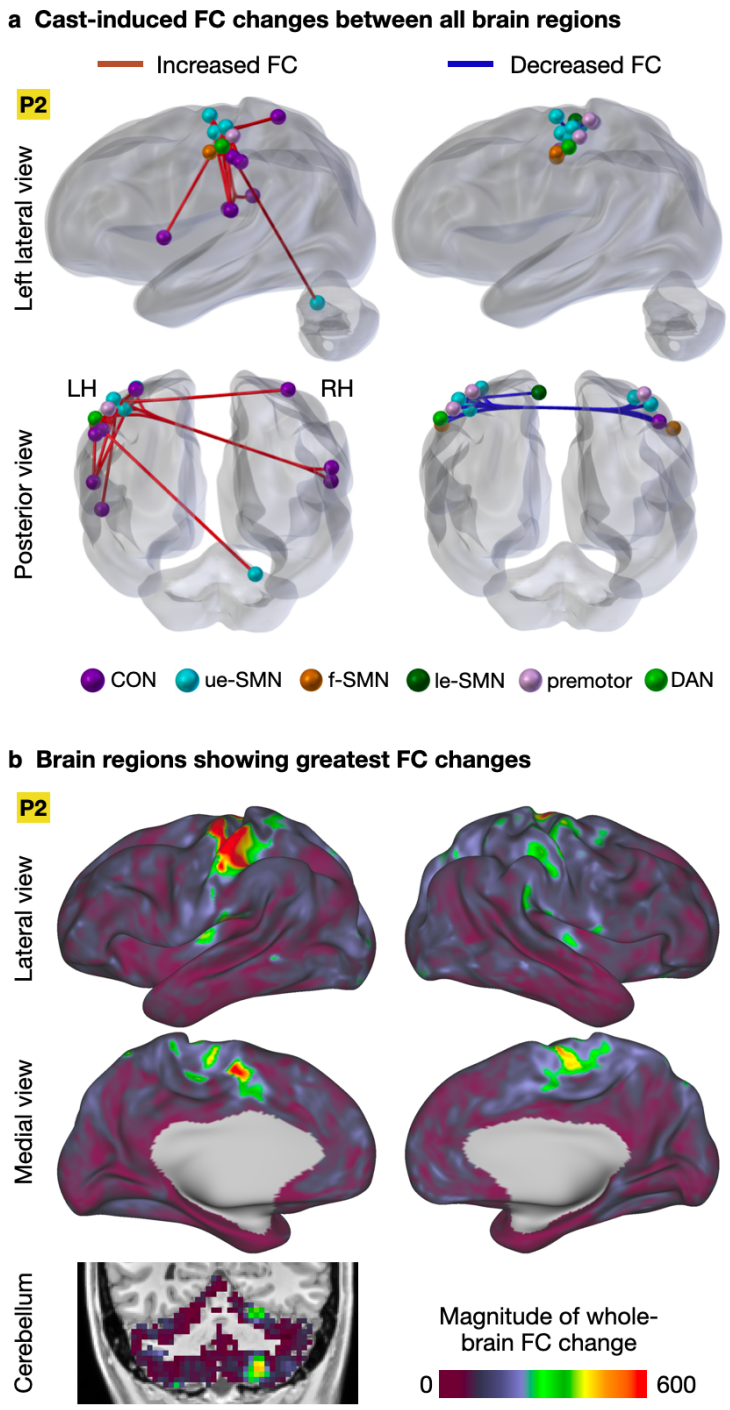

Fig. 4 | Whole-brain Analyses of Disuse-driven Functional Connectivity (FC) Changes. a, Changes in functional connectivity (FC) were computed for all pairs of cortical, subcortical and cerebellar parcels (mean Cast FC – mean Pre FC). The 50 most altered functional connections (top 25 increases, top 25 decreases) are shown for an example participant (P2; all participants, Supplementary Fig. 3). **b,** For each vertex/voxel, the magnitude of whole-brain FC change was computed as the sum of squared FC changes between that vertex and every other gray-matter vertex/voxel. Shown for an example participant (P2; all participants shown in Supplementary Fig. 4).

143 In both cases, we compared FC between L-
144 SM1$_{ue}$ and the left dorsal anterior cingulate
145 cortex (L-dACC; Fig. 5a), a key node of the
146 CON, in cast and no-cast conditions. As
147 suggested by the whole-brain network
148 analyses (Fig. 3b), FC between L-SM1$_{ue}$ and
149 L-dACC was significantly increased during
150 the cast period (Fig. 5b). When participants
151 wore casts during scans, but were not casted
152 during their daily lives, no changes in FC
153 were observed (Fig. 5c). This control
154 experiment indicated that increased FC
155 between the disused motor circuitry and the
156 CON depended on participants' recent
157 history of disuse, not their current state of
158 casting.

159

160 **Network-Specific Connectivity Changes**
161 **Reflect Spontaneous Activity Pulses**

162 Increases in FC with L-SM1$_{ue}$ showed a
163 similar anatomical distribution to the
164 spontaneous activity pulses we described
165 previously[30] (Fig. 6a-b). Additionally, FC
166 between L-SM1$_{ue}$ and the CON was highly
167 correlated with the number of pulses detected in L-SM1$_{ue}$ during each scan (Fig. 6c; P1:

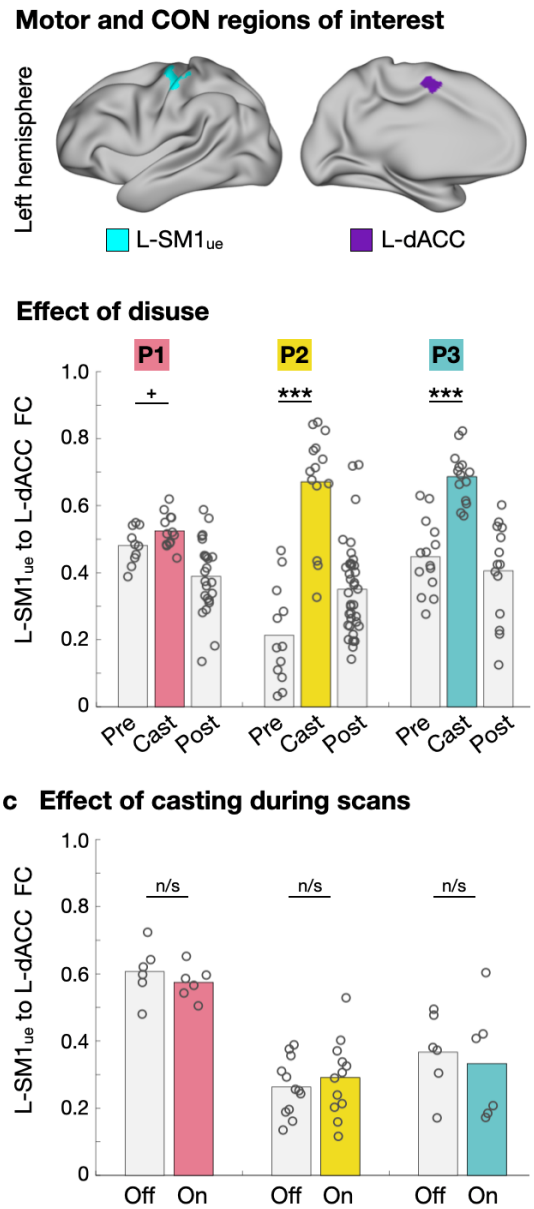

Fig. 5 | Connectivity between Disused Somatomotor Cortex and Cingulo-opercular Network during Disuse and Temporary Casting. a, Example regions of interest (ROIs) in the left primary somatomotor cortex (L-SM1$_{ue}$) and the left dorsal anterior cingulate cortex (L-dACC). **b,** Functional connectivity (FC) measured between L-SM1$_{ue}$ and L-dACC before (Pre), during (Cast) and after casting (Post). Two participants (P2 and P3) show a significant increase in FC during the cast period $^{+}P < 0.1$, $^{*}P < 0.05$, $^{***}P < 0.001$. (**C**) FC measured between L-SM1$_{ue}$ and L-dACC during both conditions of the control experiment: without casting (Off) and with temporary casts during scans (On). No changes in FC were observed.

168 r=0.74, P<0.001; P2: r=0.57, P<0.001; P3: r=0.73, P<0.001). These observations led us to

169 suspect that FC between L-SM1$_{ue}$ and the CON was increased during the cast period because

170 both regions showed synchronized spontaneous activity pulses.

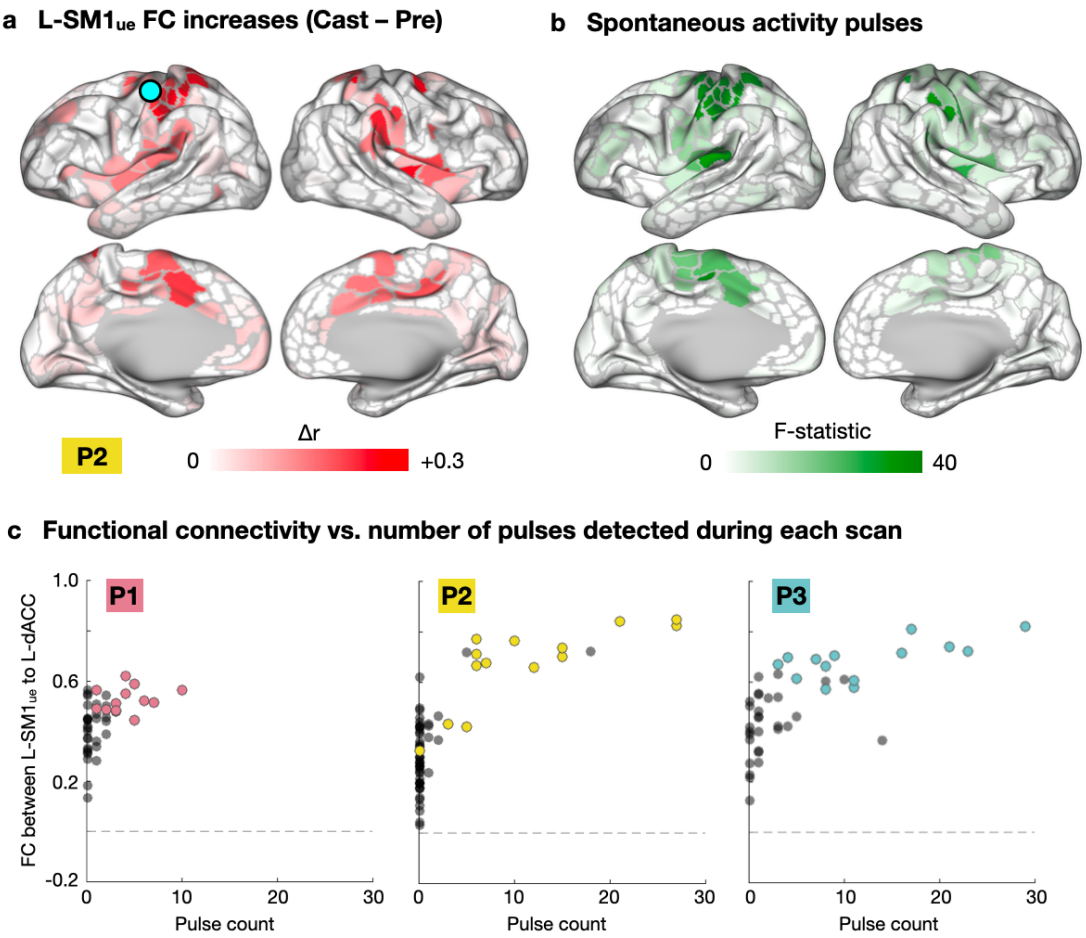

Fig. 6 | Relationship of Spontaneous Activity Pulses to Functional Connectivity (FC) Changes. a, Increases in FC with the disused somatomotor cortex (L-SM1$_{ue}$) during casting, repeated from Figure 3b for reference. **b,** Analysis of variance (ANOVA) showing regions with spontaneous activity pulses. ANOVA F-statistic was correlated with FC change in each parcel (P1: r = 0.16, P < 0.001; P2: r = 0.29, P < 0.001; P3: r = 0.06, P = 0.12). **c,** Relationship of FC between L-SM1$_{ue}$ and the dorsal anterior cingulate cortex (dACC; cingulo-opercular network (CON)) vs. the number of pulses detected. Each dot represents one 30-minute scan. Colored dots represent scans during the cast period. For all participants, FC between L-SM1$_{ue}$ and dACC was significantly correlated with the number of pulses detected (P1: r=0.74, P<0.001; P2: r=0.57, P<0.001; P3: r=0.73, P<0.001).

171

172 To test if spontaneous activity pulses could explain observed increases in FC, we implemented

173 a pulse censoring strategy, in which frames surrounding each detected pulse (13.2 s before –

174 17.6 s after each pulse peak) were excluded from FC calculations (Fig. 7a). This approach is

similar to the censoring strategy commonly used to correct the effects of head-motion on FC[31]. Censoring pulses partially reduced the FC changes observed during casting (Fig. 7b; P1 -55%, P = 0.14; P2: -28%, P = 0.02; P3: -21%, P = 0.04; one-tailed t-test). Additionally, the spatial pattern of FC changes caused by pulse censoring (Censored – Uncensored; Fig. 7c, Supplementary Fig. 4) was negatively correlated with FC changes during casting (P1: r = -0.35, P < 0.001; P2: r = -0.90, P < 0.001; P3: r = -33, P < 0.001).

Censoring pulses did not entirely eliminate the effect of casting on FC. The residual effect of casting after pulse censoring was negatively spatially correlated with the effects of pulse censoring (Supplementary Fig. 4; P1: spatial correlation, r = -0.23, P < 0.001; P2: r = -0.76, P < 0.001; P3: r = -0.18; P < 0.001), suggesting that the residual effect may have been driven by additional pulses that were too small to distinguish from ongoing spontaneous activity fluctuation. Pulses showed a wide distribution of magnitudes (Fig. 8a; range: 0.4 – 1.2% rs-fMRI signal change). Because pulses were detected using a threshold-based approach[30], pulses smaller than

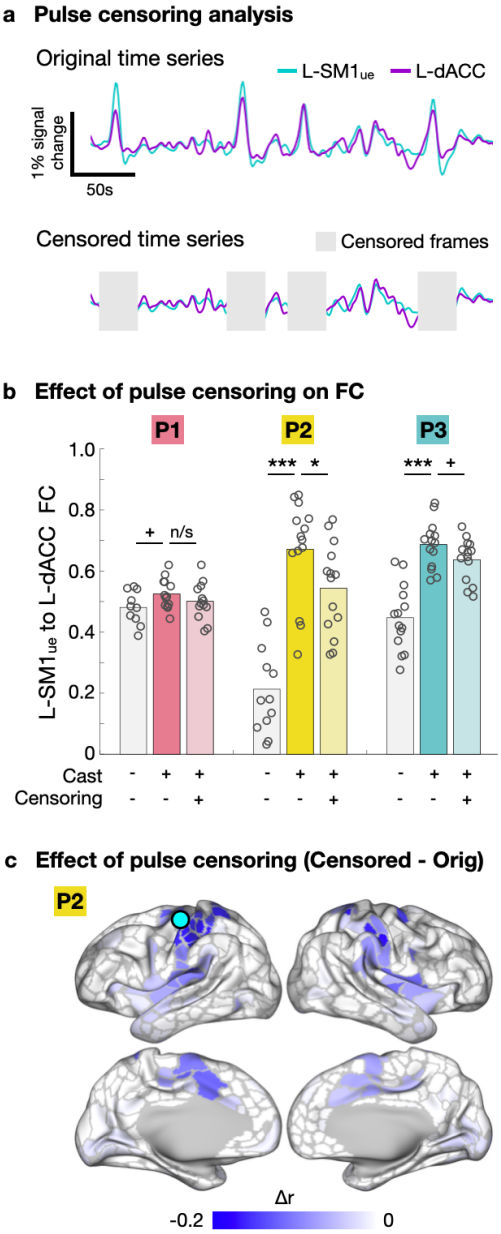

Fig. 7 | Censoring Pulses from Functional Connectivity (FC) Measurements. a, Schematic explaining censoring approach used to remove detected pulses from FC calculation. **b,** Censoring pulses partially reduced the difference between Pre and Cast scans. $^{+}$P < 0.1, *P < 0.05, ***P < 0.001. **c,** Subtraction map showing reductions in L-SM1$_{ue}$ FC due to pulse censoring. The spatial pattern of FC changes due to pulse censoring was significantly negatively correlated with FC changes during casting (P1: r = -0.35, P < 0.001; P2: r = -0.90, P < 0.001; P3: r = -0.33, P < 0.001)

0.4% fMRI signal change could not be detected and censored. To test if smaller pulses that escaped detection could explain the residual increased FC between L-SM1$_{ue}$ and L-dACC after pulse censoring, we simulated a full distribution of pulse magnitudes by adding the mean pulse time series from L-SM1$_{ue}$ and L-dACC to the baseline rs-fMRI signals recorded from these regions prior to casting (Fig. 8b). Simulated pulse magnitudes were drawn from a log-normal distribution, fit to the magnitude distribution of detected pulses using a least-squares approach (Fig. 8a; see Supplementary Fig. 5 for triangular and exponential distributions). Adding simulated pulses caused FC increases with a similar effect size (P1: Δr = +0.07, P = 0.013; P2: +0.40, P < 0.001; P3: +0.19, P < 0.001) to the FC increases observed during casting (Fig. 8c). Applying the same pulse censoring strategy described above to the simulated pulses partially reduced the increases in FC (Fig. 8c; P1: -79%, P < 0.001; P2: -58%, P < 0.001; P3: -69%, P < 0.001), similar to the effect of

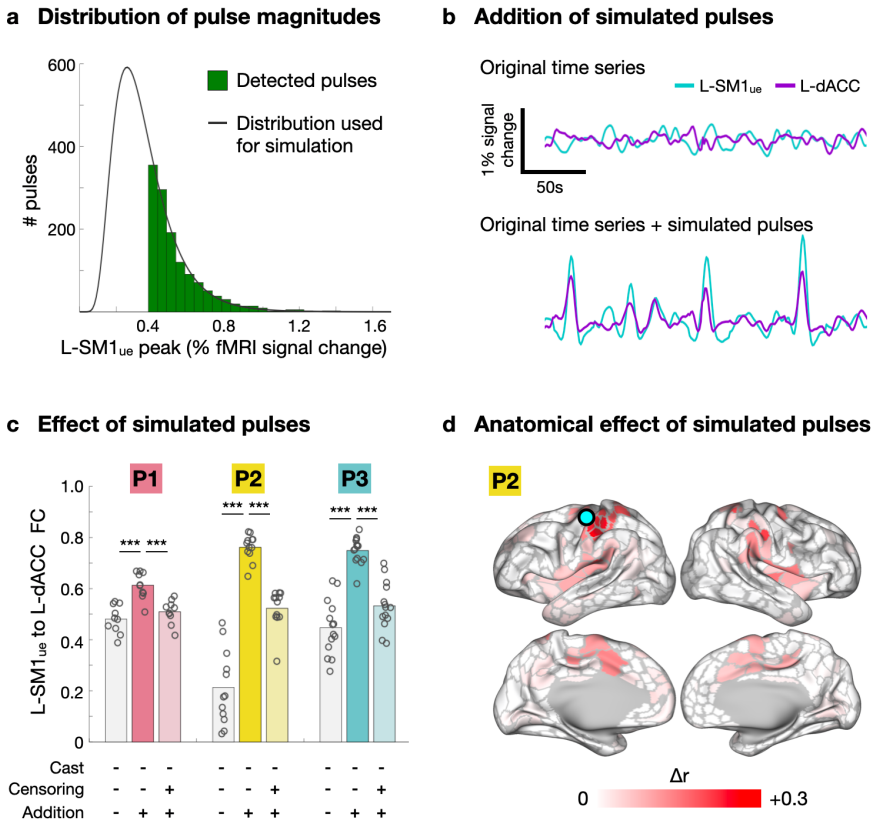

Fig. 8 | Addition of Simulated Pulses. a, Histogram of pulse magnitudes (peak fMRI signal), pooled across participants. A log-normal distribution (black line) was fit to the data using a least-squares approach. **b,** *Top:* Example resting-state functional MRI (rs-fMRI) signals from disused motor cortex (L-SM1$_{ue}$) and the dorsal anterior cingulate cortex (L-dACC) recorded prior to casting (Pre). *Bottom:* Same time series with simulated pulses added at random time points. Simulated pulse magnitudes were drawn from the full distribution shown in panel C. **c,** Adding simulated pulses increased FC between L-SM1$_{ue}$ and L-dACC (***P<0.001). Censoring simulated pulses partially reduced FC increases (***P<0.001). **d,** Subtraction map showing increases in L-SM1$_{ue}$ FC caused by simulated pulses in an example participant (P2; all participants, Supplementary Fig. 7).

225 pulse censoring on the actual data (Fig. 7b). Adding simulated pulses to all brain regions,
226 using mean pulse time series specific to each region, recreated the anatomical distribution of
227 FC changes observed during casting (Fig. 7d, Supplementary Fig. 6; P1: $r = 0.44$, $P < 0.001$;
228 P2: $r = 0.95$, $P < 0.001$; P3: $r = 0.64$, $P < 0.001$). Thus, pulse with a full distribution of
229 magnitudes could account for observed FC changes during casting and the partial reversal of
230 FC changes after pulse censoring.
231
232 We also utilized the pulse censoring and pulse addition analyses to test if pulses could explain
233 observed decreases in FC within the somatomotor system. Pulse censoring did not
234 significantly reverse the decrease in FC between L-$SM1_{ue}$ and R-$SM1_{ue}$ observed during the
235 cast period (Supplementary Fig. 7). Adding simulated pulses to baseline time series decreased
236 FC between L-$SM1_{ue}$ and R-$SM1_{ue}$, but this effect was much smaller than that observed during
237 casting (Supplementary Fig. 7).
238

239 ## Discussion

240 **Disuse Drives Plasticity of Functional Networks**

241 Daily 30-minute scans of rs-fMRI before, during, and after casting revealed that disuse not only
242 causes plasticity within the primary motor cortex[3,30], but also increased functional connectivity
243 between disused circuits and executive control regions in the CON. These increases in FC
244 would have been difficult to observe using the focal recording techniques traditionally
245 employed to study plasticity. Thus, understanding the total impact of disuse on brain function
246 will require consideration of plasticity at multiple spatial scales. Future studies using positron
247 emission tomography (PET) to monitor local metabolic changes will further strengthen the
248 bridge between whole-brain plasticity and molecular mechanisms[32].
249

250 The high degree of network specificity seen in disuse-driven plasticity is a powerful
251 demonstration of the validity of individual-specific rs-fMRI network parcellations. It could have
252 been the case that casting produced a complex pattern of FC changes involving many brain
253 systems. Instead, we found that virtually all of the regions showing increased connectivity with
254 the disused motor cortex belonged to a single network, the CON. Large-scale functional
255 networks seem to be a fundamental unit of brain organization, important not only for
256 understanding patterns of activation during cognitive processes, but also for understanding
257 whole-brain patterns of plasticity.
258

259 **Spontaneous Activity Pulses Alter Functional Connectivity**

260 The network-specific increases in FC between the disused L-SM1$_{ue}$ and the CON likely reflect
261 the emergence of synchronized spontaneous activity pulses in these regions during casting.
262 FC is a measurement of the temporal correlation of spontaneous activity between brain
263 regions. Two complementary analyses (pulse censoring and pulse addition) suggested that
264 pulses contributed to increases in measured FC between disused motor regions and the CON.
265 Many studies have reported increased FC in neuropsychiatric conditions, e.g., Parkinson's
266 disease[33] and Major Depressive Disorder[34]. Perhaps some previously reported FC increases
267 could reflect spontaneous activity pulses, similar to those caused by limb disuse. Going
268 forward, spontaneous activity pulses, and the network-specific FC changes they produce,
269 could serve as a biP3ker of recent disuse and states of heightened plasticity[35].
270

271 Decreases in connectivity within the somatomotor system were not fully explained by
272 spontaneous activity pulses. Although the pulse addition analyses showed that spontaneous
273 activity pulses could contribute to decreases in connectivity observed during casting, both the
274 pulse censoring and pulse addition analyses suggested that at least part of the observed

decrease in connectivity occurred independently of pulses. Loss of typical co-activation of L-SM1$_{ue}$ and R-SM1$_{ue}$ during daily behavior[30] likely contributed to casting-driven connectivity decreases, consistent with the widely held hypothesis that FC is maintained by a Hebbian-like mechanism that depends on co-activation of brain regions during behavior[18,32,36-38].

Disuse Impacts Cingulo-opercular Network (CON) Important for Executive Control

The importance of control systems in the human brain has been recognized for several decades[5], but our understanding of these systems has changed dramatically over time and continues to evolve[39]. Disentangling the roles of two functional networks mediating executive control, the cingulo-opercular and frontoparietal networks, has relied largely on complex task designs such as task-switching[20] and slow-reveal paradigms[40]. Here, we have demonstrated that a new approach, whole-brain precision functional mapping combined with anatomically specific disuse paradigms, can shed new light on the network interactions that support human cognition and behavior. Although the brain contains several suspected cognitive control networks beyond the CON, such as the frontoparietal (FPN), dorsal attention (DAN), ventral attention (VAN) and salience (SAL) networks, disused motor regions only increased FC with the CON. The CON is thought to initiate goal-directed behaviors and maintain executive control settings in relation to task objectives[17,18]. The increased FC between disused L-SM1$_{ue}$ and the CON during casting suggests either 1) circuits within the CON were also disused during casting, 2) the CON helps to maintain disused motor circuitry, or 3) spontaneous activity pulses can spread along functional connections to neighboring brain regions in network space.

Spontaneous activity pulses may have emerged in the CON because its use was also reduced during casting. We previously suggested that spontaneous activity pulses found in motor regions may have been caused by disuse-driven changes in local inhibitory physiology[30,41].

300 The CON is generally thought to represent task sets, abstract parameters and motor programs
301 governing goal-driven behaviors[17,18]. Task sets can be applied to multiple motor effectors (e.g.,
302 right hand, left index finger, etc.), so it would be reasonable to think that casting one extremity
303 would not cause disuse of the CON. However, at least two sets of circuits within the CON may
304 have been disused during casting: circuits that represent bimanual behaviors and circuits that
305 convey task sets to effector-specific downstream regions (e.g., L-SM1$_{ue}$). During casting, many
306 of the task sets previously used to control the dominant upper extremity (e.g., inserting a key
307 into a lock) could have been used to control the non-dominant extremity. However, task sets
308 requiring bimanual coordination (e.g., fastening a belt) could not be applied to an alternative
309 set of motor effectors and may have become disused. Another set of CON circuits that may
310 have been disused are the circuits that convey task set information to effector-specific brain
311 regions. The CON contains both somatotopically organized regions (e.g., SMA, SII) and non-
312 somatotopic regions (e.g., anterior insula). Recent work shows that the SMA and SII, as well
313 as regions of the basal ganglia, may act as hubs that connect the rest of the CON to the
314 somatomotor network[26,42]. Such circuits could potentially undergo disuse during casting of one
315 extremity.
316
317 An alternative possibility is that inputs from the CON to L-SM1$_{ue}$ served a homeostatic function
318 during disuse, helping to maintain motor circuits that are typically maintained through active
319 use. We previously suggested that spontaneous activity pulses may help to maintain the
320 organization of disused brain circuits[30]. Perhaps pulses are triggered by the CON, which is the
321 system typically responsible for initiating activation of the somatomotor network[17].
322
323 Spontaneous activity pulses may also have originated in the disused somatomotor circuits and
324 spread along functional connections to brain regions that were not affected by casting. The

CON is immediately adjacent to the somatomotor network in network space (Fig. 3a). Previous work in mice found that spontaneous activity bursts in somatosensory cortex, caused by local pharmacogenetic suppression of inhibitory interneurons, spread to other functionally connected regions not targeted by the experimental manipulation[43]. An interesting question for future research is whether the CON would show spontaneous activity pulses following disuse of brain systems other than the somatomotor network, such as networks supporting visual and auditory processing, spatial navigation, or social cognition.

Two Complementary Mechanisms for Functional Network Plasticity

Extensive whole-brain imaging before, during and after casting revealed that disuse-driven spontaneous activity pulses occur not only in primary motor and somatosensory areas, but also in higher-order brain regions responsible for executive control over behavior (i.e., the CON). The emergence of spontaneous activity pulses during casting produced increases in FC that were highly focal in network space, specifically occurring between disused motor regions and the CON. Decreases in connectivity between disused motor circuits and the remainder of the somatomotor system, however, were not explained by spontaneous activity pulses. Thus, disuse may drive network plasticity through two complementary mechanisms. Decreased coactivation of brain regions during disuse might drive Hebbian-like disconnection between disused and still-active somatomotor circuits. Spontaneous activity pulses, which contributed to increased connectivity with the CON, may help preserve disused circuits for future reintegration and use. Together, these two network plasticity mechanisms—Hebbian-like and pulse-mediated—may represent a network-focal “stand-by mode” that allows the brain to isolate disused circuits while simultaneously protecting them from premature functional degradation.

Acknowledgements:
We thank Kristen M. Scheidter and Annie L. Nguyen for help in collecting MRI data and Ryan V. Raut for his comments on the manuscript. This work was supported by NIH grants NS110332 (D.J.N.), NS088590 (N.U.F.D.), TR000448 (N.U.F.D.), MH96773 (N.U.F.D.), MH122066 (N.U.F.D.), MH1000872 (T.O.L.), MH112473 (T.O.L.), NS090978 (B.P.K.), MH104592 (D.J.G.), NS080675 (M.E.R.), NS098577 (to the Neuroimaging Informatics and Analysis Center); the US Department of Veterans Affairs Clinical Sciences Research and Development Service grant 1IK2CX001680 (E.M.G.); Kiwanis Neuroscience Research Foundation (N.U.F.D.); the Jacobs Foundation grant 2016121703 (N.U.F.D.); the Child Neurology Foundation (N.U.F.D.); the McDonnell Center for Systems Neuroscience (D.J.N., T.O.L., A.Z., B.L.S., and N.U.F.D.); the McDonnell Foundation (S.E.P.), the Mallinckrodt Institute of Radiology grant 14-011 (N.U.F.D.); the Hope Center for Neurological Disorders (N.U.F.D., B.L.S., and S.E.P.).

Author Contributions:
D.J.N., T.O.L., C.R.H., A.Z.S., and N.U.F.D. designed the study. D.J.N., C.R.H., J.M.H., M.O., and N.U.F.D. collected the data. D.J.N. and E.M.G. analyzed the data. D.J.N., E.M.G., T.O.L., N.A.S., D.F.M., S.J.G., A.Z., A.N.N., B.A., A.R.C., B.P.K., D.J.G., M.E.R., S.E.P., A.Z.S., and N.U.F.D. interpreted the results. D.J.N. and N.U.F.D. wrote the manuscript with input from all other authors.

Declaration of interests:
The authors declare the following competing financial interest: N.U.F.D. is co-founder of NOUS Imaging.

METHODS

349 ***Human Participants***

350 Participants were three healthy, adult volunteers. Details are described in Newbold *et al.*[30].

351 ***Experimental Intervention***

352 We constrained the dominant upper extremity for two weeks by fitting each participant with a fiberglass
353 cast. Casts extended from just below the shoulder to past the fingertips. Details are described in
354 Newbold *et al.*[30].

355 ***MRI Acquisition***

356 Participants were scanned every day of the experiment for 42-64 consecutive days. We collected 30
357 minutes of resting-state functional MRI (rs-fMRI) data every day of the experiment, as well as also task
358 fMRI and T1- and T2-weighted structural scans. Acquisition parameters and procedures are detailed in
359 Newbold *et al.*[30].

360 ***MR Image Processing***

361 Preprocessing of structural and functional images, denoising of resting-state fMRI data, and cortical
362 surface projection were performed previously[30]. Fully processed data are available in the Derivatives
363 folder of the Cast-Induced Plasticity dataset on OpenNeuro (www.openneuro.org/datasets/ds002766).

364 ***ROI Selection***

365 The region of the left primary somatomotor cortex controlling the casted upper extremity (L-SM1$_{ue}$) was
366 located individually in each participant using task fMRI. Details of the task analysis and region of
367 interest (ROI) selection are described in Newbold *et al.*[30]. The L-SM1$_{ue}$ ROI was used here to generate
368 seed maps (Fig. 2, Supplementary Fig. 1), to analyze spatial specificity of whole-brain functional
369 connectivity changes (Fig. 4b, Supplementary Fig. 3) and to measure FC between L-SM1$_{ue}$ and the
370 dorsal anterior cingulate cortex (dACC) for the removable cast control experiment (Fig. 5), the pulse
371 censoring analysis (Fig. 7) and the pulse addition analysis (Fig. 8, Supplementary Fig. 5).

372 Individual-specific sets of parcels spanning the entire cerebral cortex were previously generated for
373 each participant using a functional connectivity gradient-based approach, and each parcel was
374 assigned to one of 17 canonical functional networks using a graph theory-based community detection
375 algorithm[21,30]. Cortical parcels were used here to display functional connectivity changes in anatomical
376 (Fig. 2, 3, 6-8, Supplementary Fig. 1, 2, 4, 6) and network space (Fig. 3, Supplementary Fig. 2). We
377 also generated a set of subcortical and cerebellar parcels by assigning each voxel to the functional
378 network with which it showed the strongest functional connectivity and then grouping adjacent voxels
379 with matching network assignments into parcels. Sets of cortical, subcortical and cerebellar parcels
380 were used to examine changes in FC between all pairs of brain regions (Fig. 4, Supplementary Fig. 3).

381 A subset of parcels corresponding to the left primary somatomotor cortex (L-SM1$_{ue}$) was previously
382 generated by selecting all left-hemisphere parcels assigned to the upper-extremity somatomotor
383 network, excluding any parcels that fell outside of the pre- and post-central gyri[30]. Functional
384 connections between L-SM1$_{ue}$ parcels and all other parcels were averaged to generate parcel-wise
385 seed maps (Fig. 2, 3, 6-8, Supplementary Fig. 1, 2, 4, 6) and to quantify the spatial specificity of FC
386 changes between all cortical, subcortical and cerebellar parcels (Fig. 4, Supplementary Fig. 3).

387 Individual-specific ROIs in the left dorsal anterior cingulate cortex (L-dACC) were selected using pulse
388 analysis of variance (ANOVA) maps, which were previously generated for each participant[30]. ROIs
389 were selected within a large anatomical region, automatically labeled by FreeSurfer (union of caudal
390 anterior cingulate gyrus, posterior cingulate gyrus, and superior frontal gyrus). We first located the
391 vertex showing the maximum ANOVA F-statistic and then iteratively expanded the ROI by selecting
392 neighboring vertices in descending order of F-statistic, until the ROI included 100 vertices. The L-dACC
393 ROI was used to measure FC between L-SM1$_{ue}$ and the L-dACC for pulse censoring (Fig. 7) and pulse
394 addition analyses (Fig. 8, Supplementary Fig. 6).

395 ***Functional Connectivity Measurement***

396 Mean rs-fMRI time series were extracted from the L-SM1$_{ue}$ ROI and each cortical, subcortical and

397 cerebellar parcel by averaging the time series of all vertices/voxels within the ROI/parcel. Vertex-wise
398 functional connectivity (FC) seed maps were generated for each session by computing a Pearson
399 correlation between the mean rs-fMRI time series from the L-SM1$_{ue}$ ROI and the time series from every
400 vertex. Frames with high head motion, identified previously[30], were excluded from FC calculations.
401 Vertex-wise seed maps were averaged across sessions before, during and after casting (Pre, Cast,
402 Post; Fig. 2, Supplementary Fig. 1).

403 FC between all pairs of cortical, subcortical and cerebellar parcels was measured as pairwise
404 correlations of all mean rs-fMRI time series, excluding high-motion frames, producing a correlation
405 matrix for each session. Correlation matrices were averaged over Pre, Cast and Post period. FC
406 changes during casting and recovery were computed as the differences between correlation matrices
407 (casting = Cast – Pre; recovery = Post – Cast). Full Cast – Pre differences matrices are shown in
408 Supplementary Figure 3. Parcel-wise difference seed maps showing changes in L-SM1$_{ue}$ FC during
409 casting and recovery (Fig. 2-3, Supplementary Fig. 1-2) were computed by averaging together columns
410 of the difference matrices corresponding to the L-SM1$_{ue}$ parcels (see *ROI selection,* above).

411 ***Spring Embedding***

412 Cortical parcels were displayed in network space using force-directed ("spring-embedded") graphs[44],
413 generated with Gephi (https://gephi.org/). Graph weights were taken from parcel-wise correlation
414 matrices averaged across all sessions prior to casting (Pre). Graphs were thresholded to include only
415 the top 0.2% of pairwise functional connections. We initially examined graphs using an edge threshold
416 of 0.1%, but several parcels with large FC changes were disconnected from the main graph. Thus, we
417 selected the 0.2% connection threshold to display all key findings (Fig. 3, Supplementary Fig. 2).

418 ***Functional Connectivity Changes by Network***

419 To test which functional networks showed large changes in FC with L-SM1$_{ue}$ during casting, parcel-wise
420 L-SM1$_{ue}$ seed maps were compared to individual-specific network maps. Parcel-wise L-SM1$_{ue}$
421 difference seed maps (Cast – Pre) were thresholded to contain the top 5% of parcels showing FC

422 increases/decreases. FC increases (Cast > Pre) and decreases (Cast < Pre) were examined
423 separately. The number of supra-threshold parcels in each cortical network is shown in Figure 3.
424 Alternative thresholds (top 1%, 10% and 20%) all yielded similar results. Networks containing a greater
425 number of FC increases/decreases than expected by chance were identified by comparing the number
426 of supra-threshold parcels found using each participant's true network map to the number of parcels
427 found using spatially permuted network maps (see *Statistical analyses*, below).

428 ***Whole-brain Analyses of Functional Connectivity Changes***

429 The spatial specificity of whole-brain plasticity was examined by comparing changes in FC between all
430 cortical, subcortical and cerebellar parcels to individual-specific functional network maps. We examined
431 the top 50 changes in FC (25 greatest increases and 25 greatest decreases). A change in FC between
432 two parcels was counted as involving L-SM1$_{ue}$ if either of the two parcels was an L-SM1$_{ue}$ parcel. The
433 number L-SM1$_{ue}$ changes found using each participant's true network map was compared to the
434 number of L-SM1$_{ue}$ changes found using spatially permuted network maps (see *Statistical analyses*,
435 below).

436 To examine whole-brain FC changes at a finer spatial resolution, we examined differences in FC
437 between all cortical, subcortical and cerebellar vertices/voxels. We computed the magnitude of whole-
438 brain FC change between each vertex/voxel as the sum of squared FC changes between that
439 vertex/voxel and every other gray-matter vertex/voxel (Fig. 4, Supplementary Fig. 3). We tested if
440 whole-brain FC change was higher in L-SM1$_{ue}$ than in the rest of the brain by comparing the mean
441 magnitude of whole-brain FC change inside of each participant's true L-SM1$_{ue}$ ROI to the mean
442 magnitude of whole-brain FC change inside of spatially rotated ROIs (see *Statistical analyses*, below).

443 ***Spatial and Temporal Comparisons of Pulses and FC Changes***

444 To generate a parcel-wise map of spontaneous activity pulses, we extracted rs-fMRI time series from
445 every cortical, subcortical and cerebellar parcel surrounding each detected pulse (13.2 seconds before
446 to 17.6 seconds after each pulse peak). Pulse peaks were detected previously[30]. We then performed an

447 ANOVA on the extracted time series (Fig. 6b). The spatial distribution of ANOVA F-statistics was
448 compared to the spatial distribution of L-SM1$_{ue}$ FC changes using a Pearson correlation across parcels.

449 We also compared the number of pulses detected during each rs-fMRI scan[30] to the FC measured
450 between L-SM1$_{ue}$ and L-dACC (Fig. 5c), using a Pearson correlation.

451 ***Pulse Censoring Analyses***

452 To assess the contribution of large, detectable spontaneous activity pulses (>0.4% rs-fMRI signal
453 change) to FC changes observed during casting, frames surrounding each pulse (13.2 seconds before
454 to 17.6 seconds after each pulse peak) were excluded from FC calculations. Pulse detection criteria
455 were identical to those used previously [30]. We plotted FC measured between L-SM1$_{ue}$ and L-dACC
456 during each session before casting (Pre), during casting (Cast) and during casting with pulses excluded
457 (Cens; Fig. 7b). We compared Cast vs. Pre FC measurements and Cens vs. Cast FC measurements
458 using t-tests (see *Statistical analyses*, below). We also generated difference seed maps showing FC
459 changes between L-SM1$_{ue}$ and all cortical parcels due to censoring (Cens – Cast; Fig. 7c,
460 Supplementary Fig. 4).

461 ***Pulse Addition Analyses***

462 To assess the contribution to FC changes of pulses with a hypothetical full magnitude distribution,
463 including pulses that were too small (<0.4% rs-fMRI signal change) to distinguish from ongoing
464 spontaneous activity fluctuations, we created simulated rs-fMRI time series containing a full distribution
465 of pulses. We first generated a histogram showing the magnitude distribution of detected pulses.
466 Magnitudes were grouped into bins with a width of 0.5%-signal-change. We then fit a log-normal
467 distribution to the observed pulse magnitudes using a least-squares approach (Fig. 8a). This provided
468 an estimate of the full pulse magnitude distribution, including pulses that were too small to detect. We
469 then added the mean pulse time series to the baseline (Pre) rs-fMRI time series, drawing pulse
470 magnitudes from the full log-normal distribution (example shown in Fig. 8b). The number of pulses
471 added was selected so that the number of large pulses (>0.4% signal change) would match the number

472 of pulses detected in each participant in an average Cast scan. We then computed FC of the baseline
473 time series (Pre) and the time series with added pulses (Sim; Fig. 8c). Finally, we applied the same
474 pulse censoring strategy described above to the simulated time series and computed FC after
475 censoring (Cens; Fig. 8c). Because pulse magnitudes were drawn from a full log-normal distribution,
476 only a portion of the added pulses were detected and censored. We compared Sim vs. Pre FC
477 measurements and Cens vs. Sim FC measurements using t-tests (see *Statistical analyses*, below). The
478 simulation and censoring procedures were repeated using triangular and exponential magnitude
479 distributions (Supplementary Fig. 5). We also generated difference seed maps showing FC changes
480 between L-$SM1_{ue}$ and all cortical parcels due to pulse simulation (Sim – Pre; Fig. 8d, Supplementary
481 Fig. 6).

482 ***Statistical Analyses***

483 All statistical tests were performed identically for each participant. Whenever appropriate, we used
484 simple parametric statistical tests:

485 - Spatial similarity between anatomical maps was tested using a Pearson correlation across
486 parcels (P1: d.f. = 566; P2: 578; P3: 624). Spatial correlations were computed between the
487 following maps:
488 - FC changes during casting (Cast – Pre) vs. FC changes during recovery (Post – Cast;
489 Fig. 2b)
490 - FC changes during casting (Cast – Pre) vs. pulse ANOVA (F-statistic; Fig. 6)
491 - FC changes during casting (Cast – Pre) vs. FC changes due to pulse censoring (Cens –
492 Cast; Fig. 7C, Supplementary Fig. 4)
493 - FC changes due to pulse censoring (Cens – Cast) vs. residual FC changes after pulse
494 censoring (Cens – Pre; Supplementary Fig. 4)
495 - FC changes during casting (Cast – Pre) vs. FC changes due to simulated pulses (Sim –
496 Pre; Fig. 8d, Supplementary Fig. 6)

- The number of pulses detected during each scan was compared to the FC measured between L-SM1$_{ue}$ and L-dACC using a Pearson correlation (P1: d.f. = 45; P2: 61; P3: 40; Fig. 6c).
- FC between L-SM1$_{ue}$ and L-dACC measured during each session of the cast period (P1: n = 13 sessions; P2: 13; P3: 14) was compared to FC during each session of the pre period (P1: n = 10; P2: 12; P3: 14) using a two-sided, unpaired t-test (P1: d.f. = 21, P2: 23, P3: 26; Fig. 7b).
- FC between L-SM1$_{ue}$ and L-dACC measured using the full time series (motion-censored only) of each session of the cast period (P1: n = 13 sessions; P2: 13; P3: 14) was compared to FC measurements of the same sessions excluding pulses (motion- and pulse-censored) using a one-sided, paired t-test (P1: d.f. = 24, P2: 24, P3: 26; Fig. 7b).
- FC between L-SM1$_{ue}$ and L-dACC measured during each session of the pre period (Pre; P1: n = 10; P2: 12; P3: 14) was compared to FC measurements of the same sessions after adding simulated pulses (Sim) using a two-sided, paired t-test (P1: d.f. = 18, P2: 22, P3: 26; Fig. 8c).
- FC between L-SM1$_{ue}$ and L-dACC measured using the full time simulated series (Sim; motion-censored only; P1: n = 10; P2: 12; P3: 14) was compared to FC measurements of the same sessions excluding pulses (motion- and pulse-censored) using a two-sided, paired t-test (P1: d.f. = 18, P2: 22, P3: 26; Fig. 8c).

When parametric statistical tests were not appropriate to test a specific hypothesis, we tested results against a null distribution generated via permutation resampling. In each case, our null hypothesis was that observed effects had no spatial relationship to ROIs/functional networks and any overlap occurred by chance. For vertex-wise ROIs, we modeled the null hypothesis by rotating the ROI around the cortical surface 1,000 times[45,46]. For functional networks, we modeled the null hypothesis by permuting the network assignments of parcels 1,000 times. Each permuted ROI/network map was used exactly as the actual map in order to compute a null distribution for the value of interest. The P-value reported for each test represents the two-sided probability that a value in the null distribution has a greater magnitude than the observed value. Permutation resampling was used to generate null distributions for the following values:

523 - Overlap of each functional network with increases in L-SM1$_{ue}$ FC during casting (Cast > Pre;
524 number of parcels in top 5%; Fig. 3b)
525 - Overlap of each functional network with decreases in L-SM1$_{ue}$ FC during casting (Cast > Pre;
526 number of parcels in top 5%; Fig. 3c)
527 - Overlap of L-SM1$_{ue}$ parcels with the 50 largest changes in FC between all pairs of cortical,
528 subcortical and cerebellar parcels (Fig. 4a, Supplementary Fig. 3)
529 - Magnitude of whole-brain FC change in the L-SM1$_{ue}$ ROI (Fig. 4b, Supplementary Fig. 3)

530 Since we tested the overlap of L-SM1$_{ue}$ FC increases/decreases with 17 different functional networks, a
531 Benjamini-Hochberg procedure was applied to correct for multiple comparisons, maintaining false
532 discovery rates < 0.05. Each of the three participants constituted a separate replication of the
533 experiment, rather than multiple comparisons, so no correction was necessary for tests repeated in
534 each participant.

535 ***Data Visualization***

536 Regions of interest and whole-brain pulse maps were shown on cortical surfaces generated by
537 FreeSurfer[47] and Human Connectome Project (HCP) Workbench software packages[48]. These images
538 were rendered using HCP Workbench[48]. Figures showing the greatest differences in functional
539 connectivity across the entire brain in inflated anatomical space (Fig. 4, Supplementary Fig. 3) were
540 rendered using Blender, a free and open-source 3D modeling software package (www.blender.org). To
541 make the large number of changed connections included in these images visually compact,
542 connections following similar spatial trajectories were drawn toward each other using a previously
543 published mean-shift edge bundling algorithm[49]. All other figures were produced using Matlab
544 (www.mathworks.com).

545 ***Data Availability***

546 This study used our previously published dataset[30], available on the OpenNeuro database
547 (www.openneuro.org/datasets/ds002766).

Code Availability

All code needed to reproduce our analyses is available on Gitlab (https://gitlab.com/DosenbachGreene/cast-whole-brain).

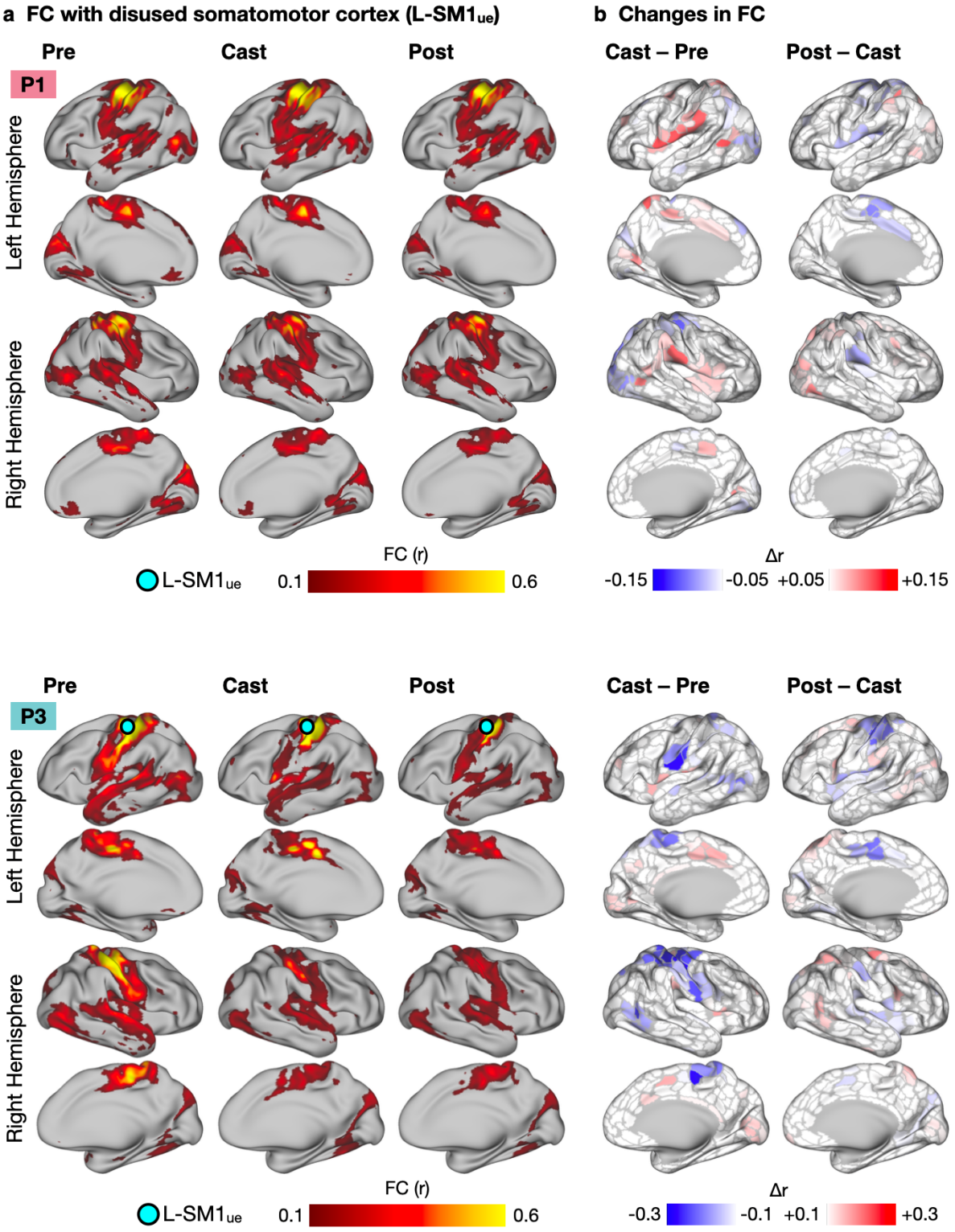

Supplementary Fig. 1: Functional Connectivity (FC) Changes Involving the Disused Somatomotor Cortex (L-SM1$_{ue}$) in Anatomical Space (All Participants). a, Seed maps showing FC between L-SM1$_{ue}$ and the remainder of the cerebral cortex in P1 (top) and P3 (bottom). Seed maps were averaged across sessions before, during and after casting (Pre, Cast, Post). **b,** Subtraction maps showing changes in FC during casting (Cast – Pre) and recovery (Post – Cast). Differences are shown on sets of 506 (P1) and 626 (P3) individual-specific cortical parcels. For P1 and P2, these parcels were previously generated and published (Gordon, 2017). We applied identical methods to generate a set of parcels for P3.

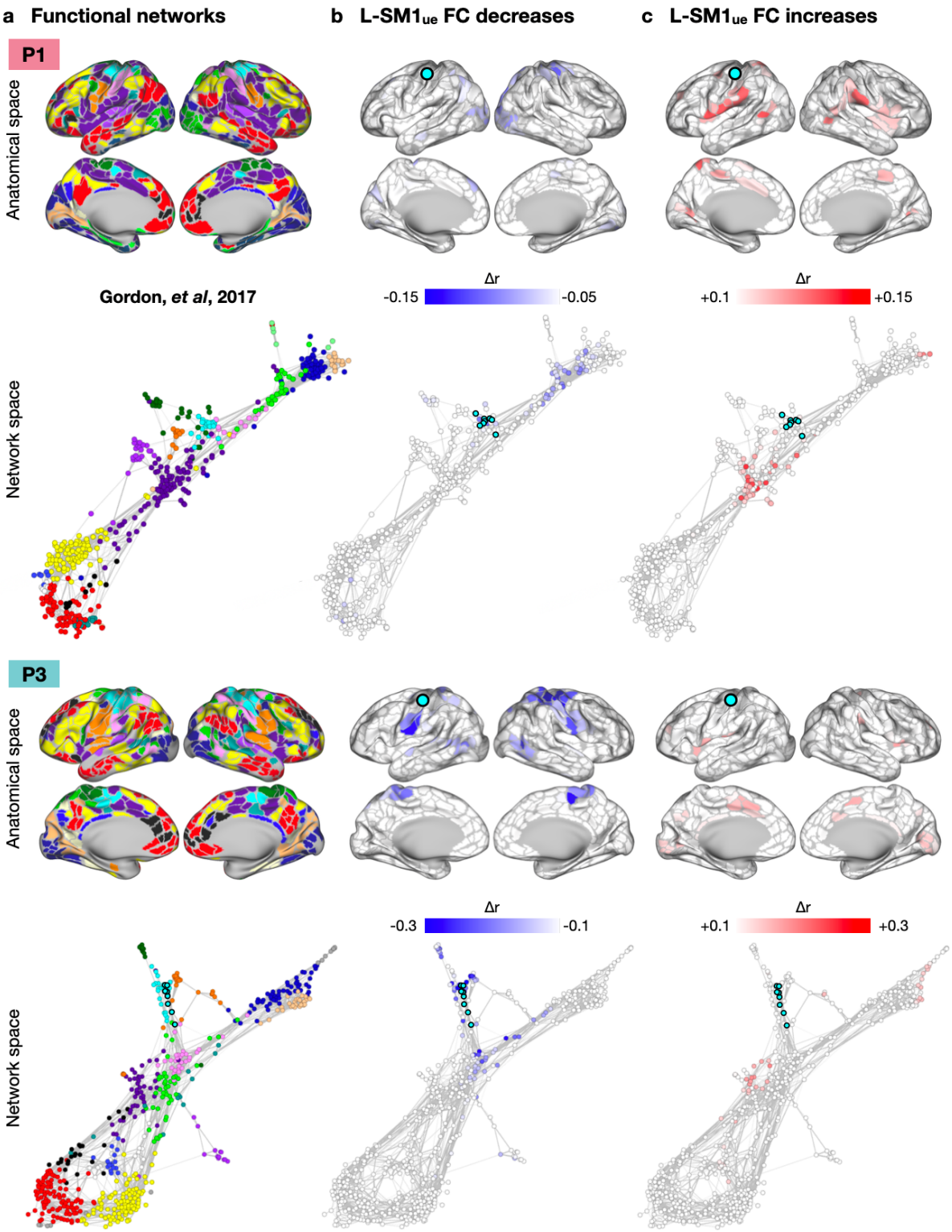

Supplementary Fig. 2: Functional Connectivity (FC) Changes Involving the Disused Somatomotor Cortex (L-SM1$_{ue}$) in Anatomical and Network Space in P1 and P3.
a, Maps of 17 canonical functional networks in P1 (top) and P3 (bottom). Networks are shown in anatomical space (inflated cortical surfaces) and network space (spring-embedded graphs based on Pre scans). See Figure 3 for network color key. **b,** Subtraction maps showing disuse-driven decreases in functional connectivity (FC) with left somatomotor cortex (L-SM1$_{ue}$) in anatomical space and network space. **c,** Subtraction maps showing disuse-driven increases in FC with L-SM1$_{ue}$ in anatomical and network space.

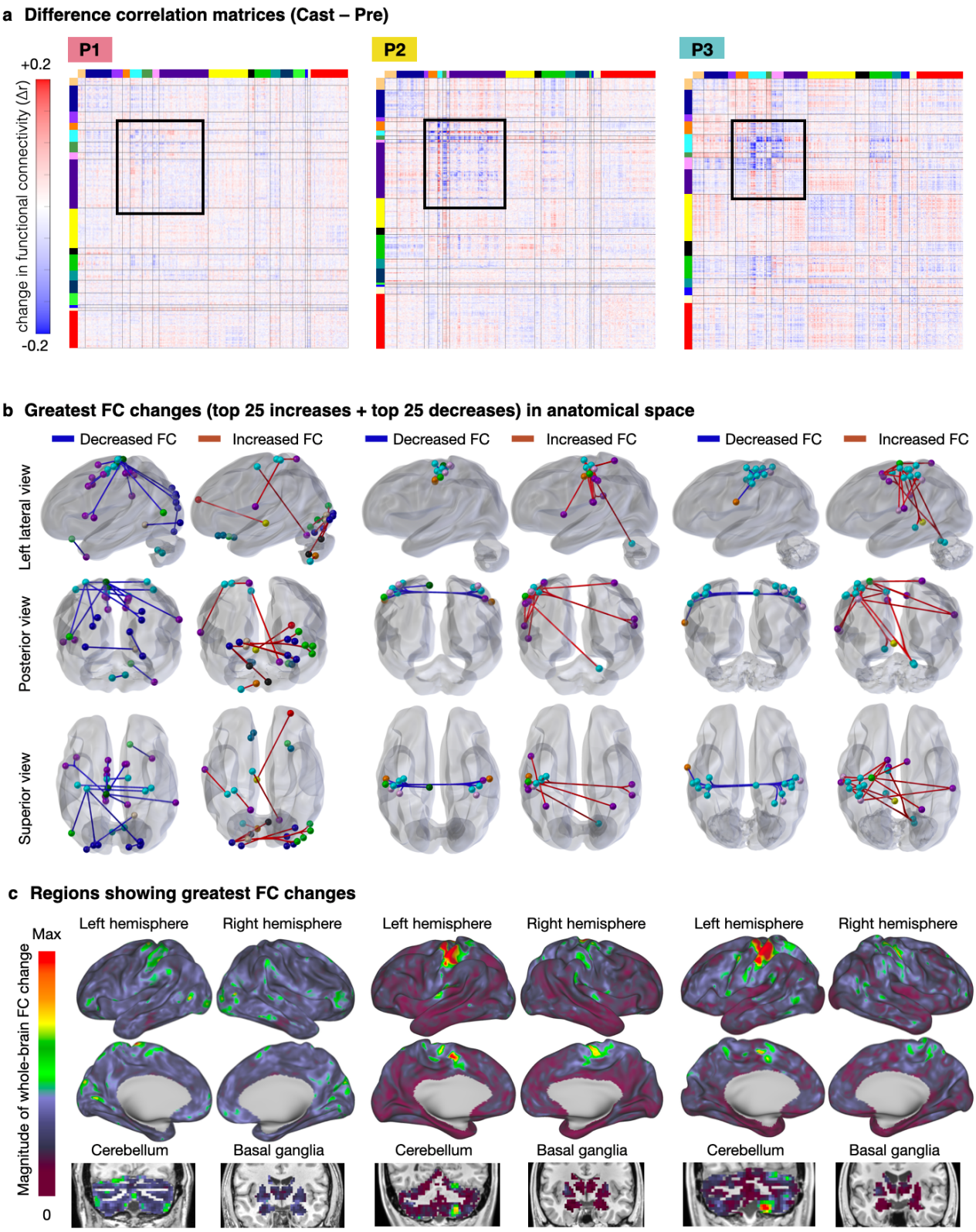

Supplementary Fig. 3: Whole-brain Patterns of Disuse-driven Plasticity. **a,** Matrices showing changes in functional connectivity (FC) between all pairs of individual specific cortical, subcortical and cerebellar parcels during casting (P1: 744 parcels, P2: 733; P3: 761**). b,** 50 largest changes in FC shown in anatomical space. **c,** Magnitude of whole-brain FC change, computed as the sum of squared FC changes between each vertex/voxel and every other gray-matter vertex/voxel

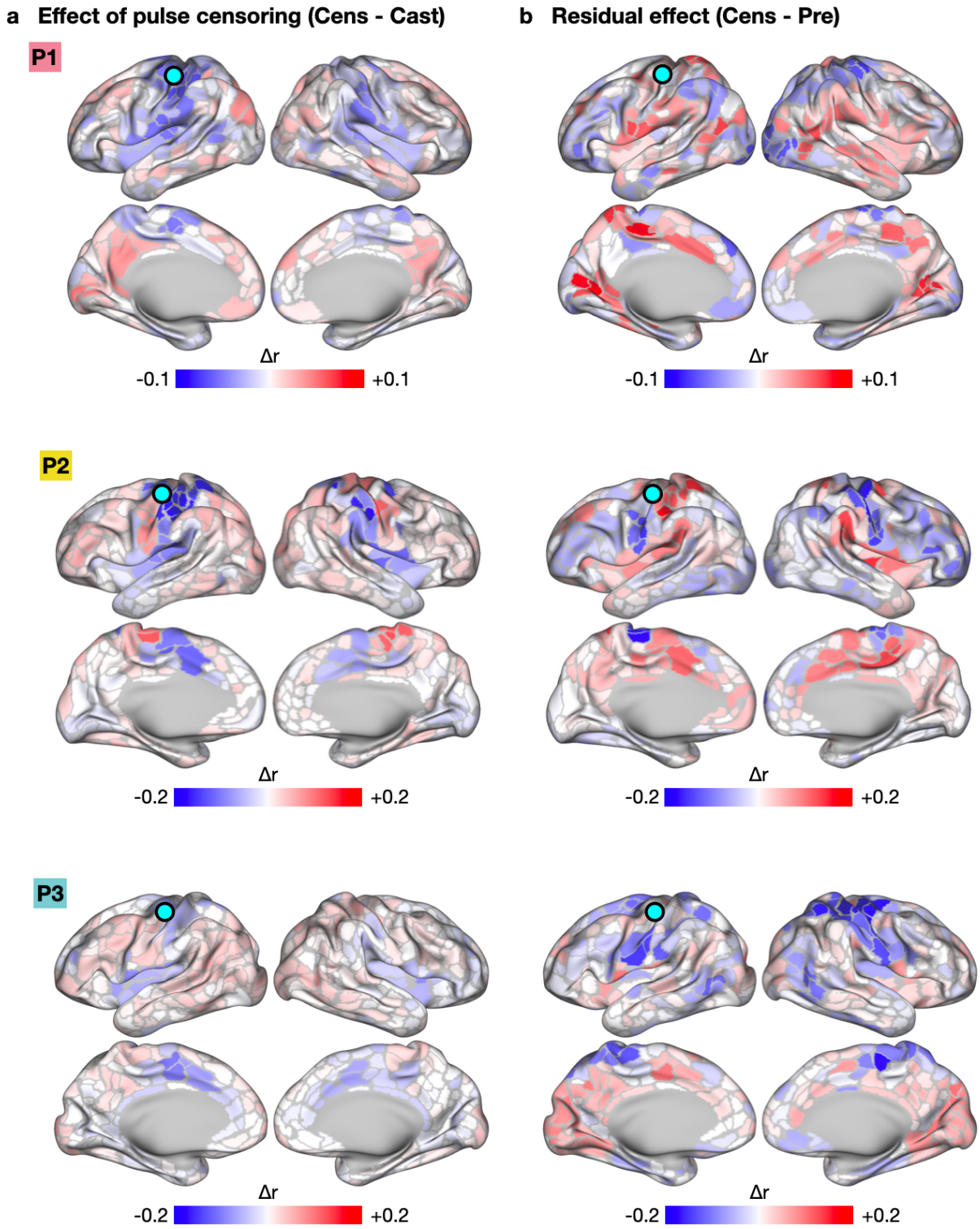

Supplementary Fig. 4: Functional Connectivity (FC) Changes Explained by Spontaneous Activity Pulses. **a,** Subtraction map showing changes in L-SM1$_{ue}$ FC due to pulse censoring. The spatial pattern of FC changes due to pulse censoring was negatively correlated with FC changes during casting (P1: r = -0.35, P < 0.001; P2: r = -0.90, P < 0.001; P3: r = -33, P < 0.001). **b,** Subtraction map showing residual FC changes during casting after pulse censoring. The spatial pattern of residual FC changes was negatively correlated with the effect of pulse censoring (P1: spatial correlation, r = -0.23, P < 0.001; P2: r = -0.76, P < 0.001; P3: r = -0.18; P < 0.001).

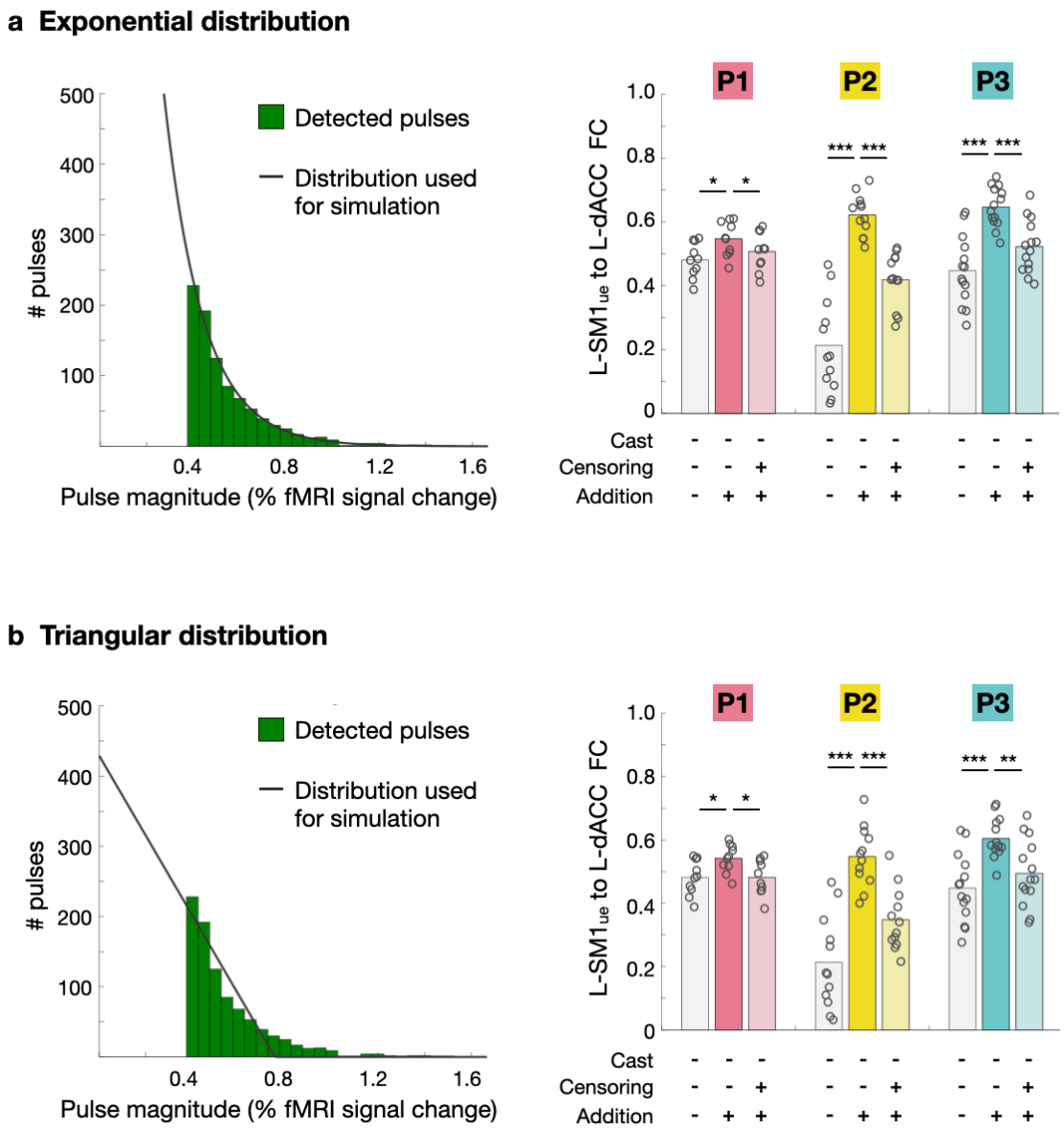

Supplementary Fig. 5: Alternative Distributions for Pulse Magnitudes. a, Exponential distribution. *Left:* Histogram of pulse magnitudes (peak fMRI signal), pooled across all participants. An exponential distribution (black line) was fit to the data using a least-squares approach. *Right:* Adding simulated pulses, with magnitudes drawn from the exponential distribution, increased FC between L-SM1$_{ue}$ and L-dACC. Censoring simulated pulses partially reduced FC increases. *P<0.05, ***P<0.001. **b,** Triangular distribution. *Left:* Histogram of pulse magnitudes (peak fMRI signal), pooled across all participants. A linear distribution (black line) was fit to the data using a least-squares approach. *Right:* Adding simulated pulses, with magnitudes drawn from the linear distribution, increased FC between L-SM1$_{ue}$ and L-dACC. Censoring simulated pulses partially reduced FC increases. *P<0.05, **P<0.01, ***P<0.001.

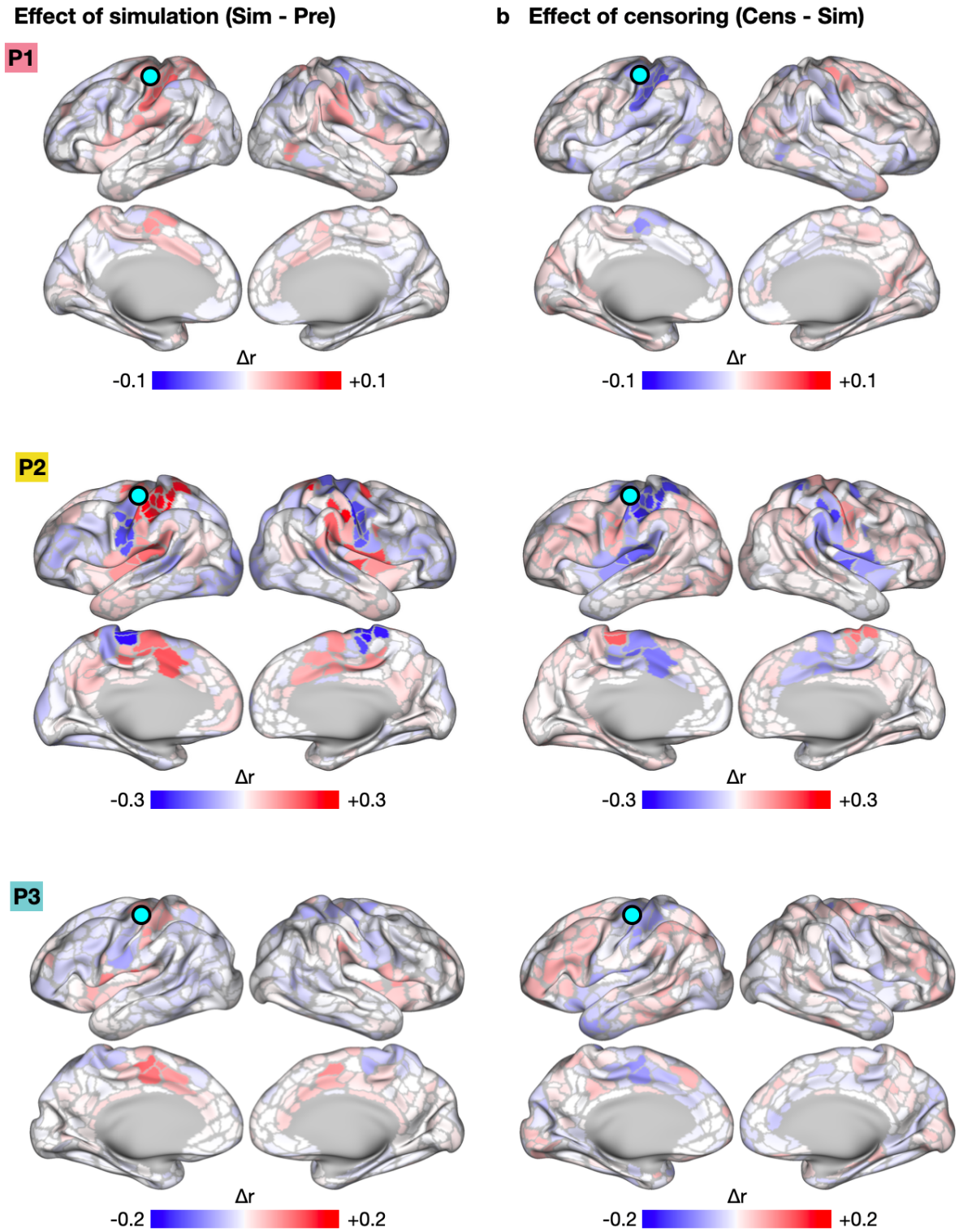

Supplementary Fig. 6: Functional Connectivity (FC) Changes Caused by Simulated Spontaneous Activity Pulses (All Participants). a, Subtraction map showing changes in L-SM1$_{ue}$ FC due to addition of simulated pulses. FC changes due to pulse addition closely matched FC changes during casting (P1: spatial correlation, r = 0.44, P < 0.001; P2: r = 0.95, P < 0.001; P3: r = 0.64, P < 0.001). **b,** Subtraction map showing effect of censoring simulated pulses. Effects of censoring closely complemented the effect of pulse addition (P1: r = -0.71, P < 0.001; P2: r = -0.96, P < 0.001; P3: r = -0.69; P < 0.001).

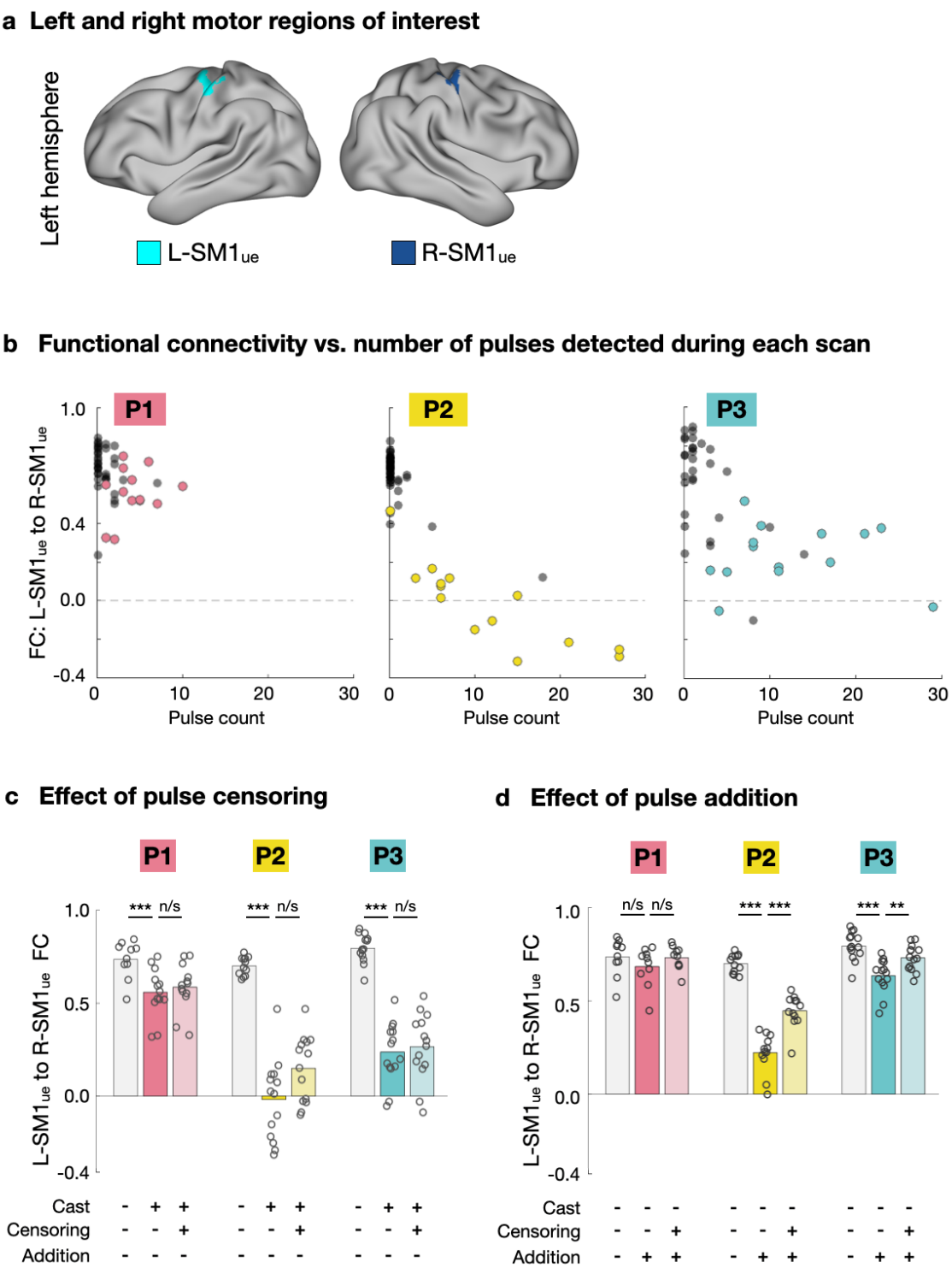

Supplementary Fig. 7: Functional Connectivity (FC) Decreases Were Not Explained by Spontaneous Activity Pulses. **a,** Example regions of interest (ROIs) in the left and right primary somatomotor cortex (L-SM1$_{ue}$ and R-SM1$_{ue}$). **b,** Relationship of FC between L-SM1$_{ue}$ and R-SM1$_{ue}$ vs. the number of pulses detected. Each dot represents one 30-minute scan. Colored dots represent scans during the cast period. For all participants, FC between L-SM1$_{ue}$ and R-SM1$_{ue}$ was significantly correlated with the number of pulses detected (P1: r=0.74, P<0.001; P2: r=0.57, P<0.001; P3: r=0.73, P<0.001). **c,** Censoring pulses did not reduce the difference between Pre and Cast scans. ***P < 0.001. **d,** Adding simulated pulses decreased FC between L-SM1$_{ue}$ and R-SM1$_{ue}$ in two participants (P2 and P3), but these decreases were much smaller than those observed during casting. ***P < 0.001. **P < 0.01.

REFERENCES

1 Wiesel, T. N. & Hubel, D. H. Comparison of the effects of unilateral and bilateral eye closure on cortical unit responses in kittens. *J Neurophysiol* **28**, 1029-1040, doi:10.1152/jn.1965.28.6.1029 (1965).

2 Merzenich, M. M. *et al.* Topographic reorganization of somatosensory cortical areas 3b and 1 in adult monkeys following restricted deafferentation. *Neuroscience* **8**, 33-55 (1983).

3 Milliken, G. W., Plautz, E. J. & Nudo, R. J. Distal forelimb representations in primary motor cortex are redistributed after forelimb restriction: a longitudinal study in adult squirrel monkeys. *J Neurophysiol* **109**, 1268-1282, doi:10.1152/jn.00044.2012 (2013).

4 Feldman, D. E. & Brecht, M. Map plasticity in somatosensory cortex. *Science* **310**, 810-815, doi:10.1126/science.1115807 (2005).

5 Posner, M. I. & Petersen, S. E. The attention system of the human brain. *Annu Rev Neurosci* **13**, 25-42, doi:10.1146/annurev.ne.13.030190.000325 (1990).

6 Raichle, M. E. *et al.* A default mode of brain function. *Proc Natl Acad Sci U S A* **98**, 676-682, doi:10.1073/pnas.98.2.676 (2001).

7 Shulman, G. L., Ollinger, J. M., Linenweber, M., Petersen, S. E. & Corbetta, M. Multiple neural correlates of detection in the human brain. *Proc Natl Acad Sci U S A* **98**, 313-318, doi:10.1073/pnas.021381198 (2001).

8 Biswal, B., Yetkin, F. Z., Haughton, V. M. & Hyde, J. S. Functional connectivity in the motor cortex of resting human brain using echo-planar MRI. *Magn Reson Med* **34**, 537-541 (1995).

9 Fox, M. D. *et al.* The human brain is intrinsically organized into dynamic, anticorrelated functional networks. *Proc Natl Acad Sci U S A* **102**, 9673-9678, doi:10.1073/pnas.0504136102 (2005).

10 Greicius, M. D., Krasnow, B., Reiss, A. L. & Menon, V. Functional connectivity in the resting brain: a network analysis of the default mode hypothesis. *Proc Natl Acad Sci U S A* **100**, 253-258, doi:10.1073/pnas.0135058100 (2003).

11 Yeo, B. T. *et al.* The organization of the human cerebral cortex estimated by intrinsic functional connectivity. *J Neurophysiol* **106**, 1125-1165, doi:10.1152/jn.00338.2011 (2011).

12 Power, J. D. *et al.* Functional network organization of the human brain. *Neuron* **72**, 665-678, doi:10.1016/j.neuron.2011.09.006 (2011).

13 Cordes, D. *et al.* Frequencies contributing to functional connectivity in the cerebral cortex in "resting-state" data. *AJNR Am J Neuroradiol* **22**, 1326-1333 (2001).

14 Lowe, M. J., Mock, B. J. & Sorenson, J. A. Functional connectivity in single and multislice echoplanar imaging using resting-state fluctuations. *Neuroimage* **7**, 119-132, doi:10.1006/nimg.1997.0315 (1998).

15 Fox, M. D., Corbetta, M., Snyder, A. Z., Vincent, J. L. & Raichle, M. E. Spontaneous neuronal activity distinguishes human dorsal and ventral attention systems. *Proc Natl Acad Sci U S A* **103**, 10046-10051, doi:10.1073/pnas.0604187103 (2006).

16 Seeley, W. W. *et al.* Dissociable intrinsic connectivity networks for salience processing and executive control. *J Neurosci* **27**, 2349-2356, doi:10.1523/JNEUROSCI.5587-06.2007 (2007).

17 Dosenbach, N. U. *et al.* Distinct brain networks for adaptive and stable task control in humans. *Proc Natl Acad Sci U S A* **104**, 11073-11078, doi:10.1073/pnas.0704320104 (2007).

18 Dosenbach, N. U., Fair, D. A., Cohen, A. L., Schlaggar, B. L. & Petersen, S. E. A dual-networks architecture of top-down control. *Trends Cogn Sci* **12**, 99-105, doi:10.1016/j.tics.2008.01.001 (2008).

19 Marek, S. & Dosenbach, N. U. F. Control networks of the frontal lobes. *Handb Clin Neurol* **163**, 333-347, doi:10.1016/B978-0-12-804281-6.00018-5 (2019).

20 Dosenbach, N. U. *et al.* A core system for the implementation of task sets. *Neuron* **50**, 799-812, doi:10.1016/j.neuron.2006.04.031 (2006).

21 Gordon, E. M. *et al.* Precision Functional Mapping of Individual Human Brains. *Neuron* **95**, 791-807 e797, doi:10.1016/j.neuron.2017.07.011 (2017).

22 Laumann, T. O. *et al.* Functional System and Areal Organization of a Highly Sampled Individual Human Brain. *Neuron* **87**, 657-670, doi:10.1016/j.neuron.2015.06.037 (2015).

23 Wang, D. *et al.* Parcellating cortical functional networks in individuals. *Nat Neurosci* **18**, 1853-1860, doi:10.1038/nn.4164 (2015).

24 Mueller, S. *et al.* Individual variability in functional connectivity architecture of the human brain. *Neuron* **77**, 586-595, doi:10.1016/j.neuron.2012.12.028 (2013).

25 Marek, S. *et al.* Spatial and Temporal Organization of the Individual Human Cerebellum. *Neuron* **100**, 977-993 e977, doi:10.1016/j.neuron.2018.10.010 (2018).

26 Greene, D. J. *et al.* Integrative and Network-Specific Connectivity of the Basal Ganglia and Thalamus Defined in Individuals. *Neuron* **105**, 742-758 e746, doi:10.1016/j.neuron.2019.11.012 (2020).

27 Braga, R. M. & Buckner, R. L. Parallel Interdigitated Distributed Networks within the Individual Estimated by Intrinsic Functional Connectivity. *Neuron* **95**, 457-471 e455, doi:10.1016/j.neuron.2017.06.038 (2017).

28 Poldrack, R. A. *et al.* Long-term neural and physiological phenotyping of a single human. *Nat Commun* **6**, 8885, doi:10.1038/ncomms9885 (2015).

29 Sylvester, C. M. *et al.* Individual-specific functional connectivity of the amygdala: A substrate for precision psychiatry. *Proc Natl Acad Sci U S A* **117**, 3808-3818, doi:10.1073/pnas.1910842117 (2020).

30 Newbold, D. J. *et al.* Plasticity and spontaneous activity pulses in disused human brain circuits. *Neuron* **In press** (2020).

31 Power, J. D., Barnes, K. A., Snyder, A. Z., Schlaggar, B. L. & Petersen, S. E. Spurious but systematic correlations in functional connectivity MRI networks arise from subject motion. *Neuroimage* **59**, 2142-2154, doi:10.1016/j.neuroimage.2011.10.018 (2012).

32 Shannon, B. J. *et al.* Brain aerobic glycolysis and motor adaptation learning. *Proc Natl Acad Sci U S A* **113**, E3782-3791, doi:10.1073/pnas.1604977113 (2016).

33 Gratton, C. *et al.* Emergent Functional Network Effects in Parkinson Disease. *Cereb Cortex* **29**, 2509-2523, doi:10.1093/cercor/bhy121 (2019).

34 Greicius, M. D. *et al.* Resting-state functional connectivity in major depression: abnormally increased contributions from subgenual cingulate cortex and thalamus. *Biol Psychiatry* **62**, 429-437, doi:10.1016/j.biopsych.2006.09.020 (2007).

35 Kucyi, A. & Parvizi, J. Pupillary dynamics link spontaneous and task-evoked activations recorded directly from human insula. *J Neurosci*, doi:10.1523/JNEUROSCI.0435-20.2020 (2020).

36 Harmelech, T. & Malach, R. Neurocognitive biases and the patterns of spontaneous correlations in the human cortex. *Trends Cogn Sci* **17**, 606-615, doi:10.1016/j.tics.2013.09.014 (2013).

37 Guerra-Carrillo, B., Mackey, A. P. & Bunge, S. A. Resting-state fMRI: a window into human brain plasticity. *Neuroscientist* **20**, 522-533, doi:10.1177/1073858414524442 (2014).

38 Lewis, C. M., Baldassarre, A., Committeri, G., Romani, G. L. & Corbetta, M. Learning sculpts the spontaneous activity of the resting human brain. *Proc Natl Acad Sci U S A* **106**, 17558-17563, doi:10.1073/pnas.0902455106 (2009).

39 Petersen, S. E. & Posner, M. I. The attention system of the human brain: 20 years after. *Annu Rev Neurosci* **35**, 73-89, doi:10.1146/annurev-neuro-062111-150525 (2012).

40 Neta, M., Nelson, S. M. & Petersen, S. E. Dorsal Anterior Cingulate, Medial Superior Frontal Cortex, and Anterior Insula Show Performance Reporting-Related Late Task Control Signals. *Cereb Cortex* **27**, 2154-2165, doi:10.1093/cercor/bhw053 (2017).

41 Wellman, C. L., Arnold, L. L., Garman, E. E. & Garraghty, P. E. Acute reductions in GABAA receptor binding in layer IV of adult primate somatosensory cortex after peripheral nerve injury. *Brain Res* **954**, 68-72 (2002).

42 Gordon, E. M. *et al.* Three Distinct Sets of Connector Hubs Integrate Human Brain Function. *Cell Rep* **24**, 1687-1695 e1684, doi:10.1016/j.celrep.2018.07.050 (2018).

43 Rosenthal, Z. P. *et al.* Local Perturbations of Cortical Excitability Propagate Differentially Through Large-Scale Functional Networks. *Cereb Cortex* **30**, 3352-3369, doi:10.1093/cercor/bhz314 (2020).

44 Jacomy, M., Venturini, T., Heymann, S. & Bastian, M. ForceAtlas2, a continuous graph layout algorithm for handy network visualization designed for the Gephi software. *PLoS One* **9**, e98679, doi:10.1371/journal.pone.0098679 (2014).

45 Gordon, E. M. *et al.* Generation and Evaluation of a Cortical Area Parcellation from Resting-State Correlations. *Cereb Cortex* **26**, 288-303, doi:10.1093/cercor/bhu239 (2016).

46 Gordon, E. M. *et al.* Default mode network streams for coupling to language and control systems. *Proc Natl Acad Sci U S A* **In press** (2020).

47 Fischl, B. FreeSurfer. *Neuroimage* **62**, 774-781, doi:10.1016/j.neuroimage.2012.01.021 (2012).

48 Marcus, D. S. *et al.* Informatics and data mining tools and strategies for the human connectome project. *Front Neuroinform* **5**, 4, doi:10.3389/fninf.2011.00004 (2011).

49 Bottger, J., Schafer, A., Lohmann, G., Villringer, A. & Margulies, D. S. Three-dimensional mean-shift edge bundling for the visualization of functional connectivity in the brain. *IEEE Trans Vis Comput Graph* **20**, 471-480, doi:44E49295-068E-4AC0-9895-94C4713B93EC (2014).